ELSEVIER

Contents lists available at ScienceDirect

# Geochimica et Cosmochimica Acta

journal homepage: www.elsevier.com/locate/gca



# Iodine incorporation into dolomite: Experimental constraints and implications for the iodine redox proxy and Proterozoic Ocean



Mohammed S. Hashim a,b,\*, Janet E. Burke c, Dalton S. Hardisty c, Stephen E. Kaczmarek a

- <sup>a</sup> Department of Geological and Environmental Sciences, Western Michigan University, Kalamazoo, MI 49008, USA
- <sup>b</sup> Department of Marine Chemistry and Geochemistry, Woods Hole Oceanographic Institution, Woods Hole, MA 02543, USA
- <sup>c</sup> Department of Earth and Environmental Sciences, Michigan State University, East Lansing, MI 48824, USA

#### ARTICLE INFO

Article history: Received 12 May 2022 Accepted 14 October 2022 Available online 20 October 2022 Associate editor: Nicholas Tosca

Keywords:
Dolomite
Iodine
Redox
Proxies
Ocean
Oxygenation
Precambrian
Proterozoic
Trace Element
Experiment

#### ABSTRACT

lodine concentrations in sedimentary carbonate minerals are used as a proxy to reconstruct the redox landscape in shallow oceans throughout Earth history. The proxy [I/(Ca + Mg)] assumes that only the oxidized form of iodine, iodate (IO3), is incorporated into carbonate minerals, and thus its presence in ancient carbonate rocks suggests their formation under oxic conditions where iodate prevails. This assumption has been experimentally tested in calcite but not in dolomite, despite dolomite being the host mineral for much of the ancient iodine record. Here, high-temperature (170-200 °C) experiments are employed to investigate the fundamental controls on iodine incorporation in dolomite. The experiments included: 1.) the dolomitization of iodine-containing aragonite sediments in iodine-free Mg-Ca-Cl solutions to explore the effects of dolomitization by reducing pore fluids and 2.) dolomitization of iodine-free aragonite in solutions containing either iodate or iodide using various concentrations and temperatures. The I/(Ca + Mg) in natural aragonite samples dolomitized in iodate-free solutions—mimicking diagenesis in anoxic pore fluids-retain only a small proportion of the original iodine. This suggest that zero or low I/(Ca + Mg) in natural dolomites could be the result of dolomite formation and/or subsequent recrystallization in anoxic pore fluids during diagenesis and does not necessarily indicate an anoxic water column. The results of the dolomitization of the iodine-free aragonite demonstrate that iodate is incorporated into dolomite, whereas iodide is not, validating the iodine proxy, and suggesting that non-zero I/(Ca + Mg) in natural dolomites likely reflect the presence of iodate, and thus free oxygen in the dolomitizing fluid. I/(Ca + Mg) in dolomite covaries with [I] in solution, thus permitting determination of a partition coefficient for iodate (Diodate). Conversely, there is no discernable effect on iodine incorporation from reaction temperature at 170-200 °C. The results also show that I/(Ca + Mg) in dolomite decreases with increasing dolomite stoichiometry (mol % MgCO<sub>3</sub>) and cation ordering, both of which increase with reaction time, suggesting that iodine content in dolomite, and thus Diodate, is a function of the chemical and structural characteristics of dolomite. Application of experimentally derived Diodate to previously published I/(Ca + Mg) values bolster interpretations that Proterozoic [IO<sub>3</sub>]—and hence likely local O2-was maintained at low levels until the Neoproterozoic Oxygenation Event, when oxygen levels became high enough to support and stabilize the accumulation of iodate in seawater.

© 2022 Elsevier Ltd. All rights reserved.

#### 1. Introduction

The emergence, evolution, and extinction of life on Earth are intimately linked to the concentration of oxygen in the atmosphere and ocean (Lyons et al., 2021). Oxygen in the ocean has been explored over multiple geologic time scales using numerous geochemical redox-sensitive proxies, one of which is the ratio of iodine to calcium and magnesium (I/Ca + Mg) in sedimentary car-

bonate minerals, such as calcite and dolomite (Lu et al., 2010). The total amount of dissolved inorganic iodine in seawater consists pri-

marily of two thermodynamically stable species: the oxidized form, iodate ( $IO_3$ ), and the reduced form, iodide ( $I^-$ ), (Wong and Brewer, 1977). While the total iodine concentration ( $\sim$ 0.45  $\mu$ M) in seawater is nearly constant owing to its relatively long residence time (300 k.y.) (Broecker and Peng, 1982), iodate and iodide concentrations are inversely correlated (Wong and Brewer, 1977; Emerson et al., 1979; Kennedy and Elderfield, 1987a, 1987b; Rue et al., 1997; Lu et al., 2010). Iodate prevails in oxic conditions and is quantitatively reduced to iodide in anoxic basins and

<sup>\*</sup> Corresponding author.

reducing pore fluids (e.g., Rue et al., 1997; Cutter et al., 2018; Morivasu et al., 2020).

The iodine proxy is based on the premise that among the two iodine species, only iodate - the oxidized form - is incorporated into carbonate minerals (Lu et al., 2010; Zhou et al., 2014). Accordingly, carbonate minerals forming under oxic conditions, where iodate prevails, should incorporate iodine. In contrast, carbonates forming under anoxic conditions, where iodide is the dominant species, are expected to lack iodine altogether (Hardisty et al., 2014; 2017). The observation that iodate is the only iodine species incorporated into carbonate minerals has been experimentally demonstrated for calcite (Lu et al., 2010; Zhou et al., 2014), but not for dolomite. Yet, the iodine proxy has been applied equally in ancient limestones and dolostones (e.g., Loope et al., 2013; Hardisty et al., 2014; Hardisty et al., 2017; Lu et al., 2017; Owens et al., 2017; Lu et al., 2018; Shang et al., 2019; Wei et al., 2019; He et al., 2020) under the implicit assumption that dolomite, like calcite, only incorporates iodate.

Dolomite is the most abundant mineral in the carbonate rock record (e.g., Given and Wilkinson, 1987; Cantine et al., 2020), especially during the Precambrian when major environmental changes and evolutionary breakthroughs occurred. Therefore, understanding iodine incorporation in dolomite is critical for using the iodine proxy in dolomite and for comparing values across various lithologies. Furthermore, the iodine content of ancient carbonates may not always reflect depositional conditions because carbonate minerals are highly susceptible to multiple stages of diagenesis. In fact, data from relatively modern carbonate settings in the Great Bahama Bank suggest that I/(Ca + Mg) ratios in aragonite and high-Mg calcite sediments decrease during diagenetic stabilization/neomorphism and dolomitization (Hardisty et al., 2017). While these data suggests that low or no iodine in dolomite does not necessarily indicate formation under anoxic conditions but may instead reflect diagenetic loss of iodine, our understanding of how diagenesis, particularly dolomitization, impacts the iodine content is far from complete.

The development of dolomite as a geochemical archive is challenging for several reasons. First, despite the abundance of dolomite throughout the rock record, it is extremely rare in Holocene sediments (Land, 1985; Budd, 1997; Machel, 2004), complicating proxy calibration and validation under natural settings. Second, laboratory experiments have been largely unsuccessful at forming dolomite at near Earth-surface temperatures (e.g., Land, 1998; Gregg et al., 2015; Kaczmarek et al., 2017), limiting proxy development under the well-controlled laboratory conditions at temperatures under which most sedimentary dolomites form. Collectively, the scarcity of dolomite in modern environments and the failure to experimentally precipitate dolomite at Earth surface temperatures leaves high-temperature (>100 °C) experiments as the major source of geochemical information on dolomite and dolomitization (e.g., Nordeng and Sibley, 1994; Malone et al., 1996; Arvidson and Mackenzie, 1999; Kaczmarek and Sibley, 2007; Kaczmarek and Thornton, 2017). Nevertheless, only a limited number of experimental studies have explored the behavior and partitioning of trace elements between the aqueous solution and dolomite (Jacobson and Usdowski, 1976; Katz and Matthews, 1977; Malone et al., 1996).

Here we use high-temperature experiments, whereby aragonite is dolomitized in Ca-Mg-Cl fluids, to explore iodine incorporation into dolomite. We first dolomitized aragonite-dominated, iodine-containing sediments from the Great Bahama Bank under fluid-buffered settings to determine the fate of iodine initially present in sediments during dolomitization. We then dolomitized iodine-free, pulverized single crystal aragonite in solutions containing either iodate or iodide of various concentrations to determine which iodine species is incorporated into dolomite and to obtain

quantitative insights into iodine partitioning between the aqueous solution and dolomite. Experiments were conducted at various reaction temperatures (170–200 °C) to assess the effect of temperature on iodine incorporation into dolomite. Finally, the experimental findings and I/(Ca + Mg) ratios from the literature were used to calculate  $[IO_3^-]$  in the shallow ocean of the Proterozoic to better understand the redox landscape during this crucial time of Earth history.

#### 2. Methods

The experiments described here involve dolomitization of natural CaCO<sub>3</sub> precursors by replacement in a fluid-buffered, closed system. That is, the experiments were conducted in a high fluid:solid ratio with no flow-through. The replacement reaction starts off with the dissolution of the CaCO<sub>3</sub> reactant followed by the precipitation of intermediate Ca-Mg-CO<sub>3</sub> phases, followed by dolomite precipitation and subsequent recrystallization. The intermediate phases are defined here based on their MgCO<sub>3</sub> content as follows: low-Mg calcite (LMC) with < 4 mol% MgCO<sub>3</sub>, high Mg calcite (HMC) with MgCO<sub>3</sub> between 4 and 20 mol%, and very high Mg calcite (VHMC) with > 20 mol% MgCO<sub>3</sub>. Dolomite is strictly used here to refer to a Ca-Mg-carbonate phase with evidence of cation ordering as indicated by the presence of ordering reflections in XRD diffractograms (Gregg et al., 2015). The following equations describe aragonite dissolution, HMC and VHMC precipitation, and dolomite precipitation, respectively, which represent the stepwise reactions that occur during replacement dolomitization:

$$CaCO_3 + CO_2 + H_2O \rightarrow Ca^{2+} + 2HCO_3^-$$
. (1)

$$(1-x)Ca^{2+} + (x)Mg^{2+} + CO_3^{2-} \rightarrow Ca_{(1-x)}Mg_{(x)}CO_3.$$
 (2)

$$Ca^{2+} + Mg^{2+} + 2CO_3^{2-} \rightarrow CaMg(CO_3)_2.$$
 (3)

# 2.1. Dolomitization experiments

Batch experiments were carried out in 23 mL Parr Teflon-lined stainless-steel acid-digestion vessels following a similar approach to that of Kaczmarek and Sibley (2011; 2014). The vessels were charged with 200 mg of a CaCO<sub>3</sub> as a solid reactant and 15 mL of an aqueous solution (Fig. 1). Vessels were then sealed and heated

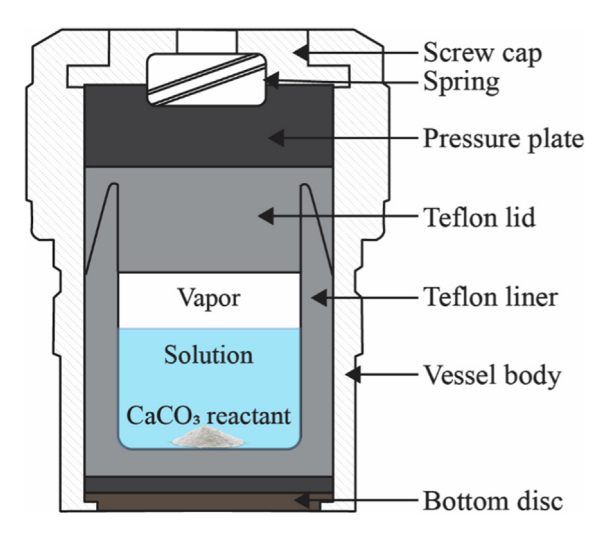


**Fig. 1.** Schematic of the Teflon lined stainless steel reaction vessel used for the dolomitization experiments.

to the desired temperature for predetermined times. Once removed from the oven, vessels were forced cooled to room temperature using compressed air. Solids were separated using a vacuum filter and dried in a desiccator.

Solid reactants were either mixed mineralogy modern carbonate sediments collected from Andros Island, Great Bahama Bank or powdered single-crystal aragonite. Modern sediments were washed with distilled water, dried overnight under room temperature, and sieved to obtain the < 63 µm size fraction. Mineralogy, as determined by powder X-ray diffraction (XRD) (described below), is 91 % aragonite, 6 % HMC, and 3 % LMC. Inductively Coupled Plasma Mass Spectrometry (ICPMS) analysis (described below) indicates that the Modern sediments contain an average I/(Ca + Mg) ratio of 8.70  $\pm$  0.19  $\mu$ mol/mol (note that the standard deviation was calculated using Excel's STDEV.P function). The aragonite was pulverized using an agate mortar and pestle, sieved to obtain the < 63 um size fraction, and annealed at 200 °C for 4 h to reduce defect-associated strain (Hashim and Kaczmarek, 2020). Mineralogy of the aragonite, as confirmed by XRD, is > 99 % aragonite and < 1 % LMC. Elemental analysis via ICPMS indicates that the single-crystal aragonite contains 0.71 mg/g Mg, 2.02 mg/g Sr (Hashim and Kaczmarek, 2020), and iodine below detection limit of instrument, which typically corresponds to I/(Ca + Mg) ratio of 0.1  $\mu$ mol/mol.

A stock solution containing 1 M Mg and 1 M Ca was prepared from laboratory grade  $\text{MgCl}_2 \cdot 6\text{H}_2\text{O}$  and  $\text{CaCl}_2 \cdot 2\text{H}_2\text{O}$  salts. The stock solution was separated into several aliquots, to which various amounts of KIO3 or KI were added to obtain solutions with the desired iodate (IO<sub>3</sub>) and iodide (I<sup>-</sup>) concentrations (Table 1). Solutions were then equilibrated with  $N_2/CO_2$  gas mixture with a known pCO<sub>2</sub> of 10<sup>-3.4</sup> (e.g., Hashim and Kaczmarek, 2021a, 2021b). The gas mixture was commercially prepared and purified by Airgas with a blend tolerance of  $\pm$  5 % and analytical accuracy of ± 1 %. Flow was controlled by a high purity dual stage regulator. The gas was flown through plastic tubing into a 100 mL gas humidifier containing deionized MilliQ water (18.2 M $\Omega$ ). The humidified gas was then bubbled into the solutions by directly inserting the plastic tubing into a 1 L beaker placed in a constant-temperature bath set to 25 ± 1 °C. A gas dispersion tube was not used to avoid possible contamination from solids trapped in the sintered glass (Morse, 1974).

Solution pH was measured using an Orion<sup>TM</sup> ROSS<sup>TM</sup> Sure-Flow combination electrode with a precision of 0.01 pH units attached to a Thermo Scientific Star Com pH meter. The pH electrode was calibrated prior to each measurement using NIST 4, 7, and 10 buffers. Temperature compensation was performed using an automatic

temperature compensator. Total alkalinity was determined by a Gran-type titration using an open cell titrator consisting of an automated syringe controlled by a computer code written in Python, an Orion combination pH electrode with automatic temperature compensator, a jacketed beaker with 250 mL capacity, a magnetic stirrer, and a stir bar. A pump was used to flow water at 25 °C through the jacketed beaker to maintain constant temperature. An N<sub>2</sub>/CO<sub>2</sub> gas mixture with a known pCO<sub>2</sub> was continuously bubbled into the cell throughout the titration process. The titrant was an HCl solution standardized using solutions of primary standard Na<sub>2</sub>CO<sub>3</sub>. The primary standard solutions were prepared using CO<sub>2</sub>-free distilled water prepared by boiling and laboratory grade Na<sub>2</sub>CO<sub>3</sub>, which was dried in an oven for 2 h and cooled in a desiccator overnight. The inflection point was determined using the Gran method (Gran, 1952). Precision of alkalinity measurements was better than 5 %.

We calculated the initial saturation state  $(\Omega)$  of the solution with respect to aragonite, LMC, and dolomite. The saturation states with respect to HMC and VHMC were not calculated due to the uncertainty in the solubility of calcite as a function of Mg content (Morse et al., 2006). The saturation state calculations were performed in PHREEQC (Parkhurst and Appelo, 2013) using log K values from a customized database covering the experimental temperature and pressure ranges generated from SUPCRTBL database (Johnson et al., 1992) based on SupPHREEQC (Zhang et al., 2020). Activity coefficients were not taken from the aforementioned database but were calculated using Pitzer ion interaction theory (Pitzer, 1991). These coefficients, along with the aqueous species concentrations, were then used to calculate activities. The activity of CO<sub>3</sub><sup>2-</sup> was calculated from the pH and carbonate alkalinity (Morse and Mackenzie, 1990), assuming that carbonate alkalinity equals total alkalinity; that is, ignoring contributions to alkalinity from non-carbonate species (e.g., boric acid, hydrogen sulfide), which is a safe assumption given that our experimental solutions are devoid of these species. The activities of Ca<sup>2+</sup> and CO<sub>3</sub><sup>2-</sup> (and Mg<sup>2+</sup> in the case of dolomite), along with temperatureand pressure-corrected mineral solubilities, were used to calculate the initial saturation state with respect to aragonite, low-Mg calcite, and dolomite (Table 1). The input file in PHREEQC included a description of the initial experimental solution, followed by solution equilibration with aragonite, which is the initial reactant used in all experiments, followed by heating to the experimental temperature. Thus, the saturation state calculations presented in Table 1 represent the initial conditions for each experiment when the solution equilibrated with the aragonite reactant before the formation of the various Ca-Mg-CO<sub>3</sub> products.

**Table 1** Experimental conditions.

Series	Reactant	Ca (M)	Mg (M)	KIO3 (μM)	KI (μM)	T (C)	P (atm)	ALK (μEq/L)	pH at 25C	pH at T	SI aragonite	SI calcite	SI dolomite
Α	Iodine-containing aragonite sediments	1	1	0	0	200	14	140.87	5.70	4.65	-2.86	-2.70	-3.93
B-1	Iodine-free single-crystal aragonite (SCA)	1	1	0	10	200	14	162.97	5.75	4.68	-2.74	-2.59	-3.71
B-2	Iodine-free SCA	1	1	0	40	200	14	166.11	5.75	4.69	-2.73	-2.57	-3.68
B-3	Iodine-free SCA	1	1	0	160	200	14	167.62	5.76	4.69	-2.72	-2.57	-3.67
C-1	Iodine-free SCA	1	1	0.2	0	200	14	138.46	5.71	4.64	-2.87	-2.72	-3.97
C-2	Iodine-free SCA	1	1	0.8	0	200	14	140.87	5.70	4.65	-2.85	-2.70	-3.93
C-3	Iodine-free SCA	1	1	10	0	200	14	137.66	5.73	4.64	-2.88	-2.73	-3.99
C-4	Iodine-free SCA	1	1	40	0	200	14	136.80	5.74	4.64	-2.89	-2.74	-4.01
C-5	Iodine-free SCA	1	1	1000	0	200	14	163.22	5.74	4.69	-2.74	-2.58	-3.69
C-6	Iodine-free SCA	1	1	10,000	0	200	14	115.03	5.71	4.63	-2.98	-2.82	-4.17
D-1	Iodine-free SCA	1	1	0.8	0	185	10	140.87	5.70	4.76	-2.59	-2.44	-3.46
D-2	Iodine-free SCA	1	1	40	0	185	10	136.80	5.74	4.75	-2.63	-2.47	-3.53
E-1	Iodine-free SCA	1	1	0.8	0	170	7	140.87	5.70	4.88	-2.33	-2.18	-3.00
E-2	Iodine-free SCA	1	1	40	0	170	7	136.80	5.74	4.87	-2.37	-2.21	-3.07

Fourteen experimental Series were performed (Table 1), each contains several individual experiments. In total, 67 experiments were conducted with at least one replicate in each Series (Supplemental Table S1). To determine the fate of iodine in CaCO<sub>3</sub> sediments during dolomitization, Series A experiments dolomitized iodine-containing carbonate sediments in an iodine-free solution. To determine which iodine species is incorporated into dolomite and to evaluate how I concentrations are partitioned from the solution during dolomitization, Series B and C experiments dolomitized iodine-free aragonite reactants in solutions with various concentrations of iodide and iodate, respectively. Series A, B, and C were conducted at 200 °C. The effects of temperature were tested in experiments that used iodine-free aragonite and KIO<sub>3</sub> solutions in Series D and E, which were conducted at 185 °C and 170 °C, respectively (Table 1).

#### 2.2. Analytical procedure

Powder XRD was used to quantify mineral abundances of the solids (reactants and products), approximate MgCO<sub>3</sub> content in products, and estimate dolomite cation ordering. Powders were prepared with an agate mortar and pestle and mounted on a Boron-doped silicon P-type zero background diffraction plates, which were placed in a Bruker D2 Phaser Diffractometer with a CuK $\alpha$  anode that has an average wavelength ( $\lambda$ ) of 1.54184 Å. Fluorite was used in all samples as an internal standard so that all XRD scans are shifted based on the fluorite 111 peak. XRD data were collected between 20 and 50°  $2\theta$  using an increment of 0.08° and a count time of 1 s. Relative abundances of aragonite, LMC, HMC, VHMC, and dolomite were determined using the ratio of aragonite 111 peak and calcite and dolomite 104 peak intensities and a correction factor determined based on known samples. MgCO3 as mol % was determined using the empirical equation of Lumsden and Chimahusky (1980), which relies on the observation that differences in ionic radii between Ca and Mg result in systematic variations in interplanar spacing:

$$MgCO_3 = 100 - (333.33 \times (d \text{ spacing}) - 911.99).$$
 (4

The accuracy of this method is within  $\sim 1~\text{mol}\%$  at low MgCO<sub>3</sub> but the error increases to  $\sim 2.5~\text{mol}\%$  at high MgCO<sub>3</sub> values (Reeder and Sheppard, 1984). Dolomite cation ordering (the arrangement of Ca and Mg in alternating cation layers within the dolomite lattice) was determined using the peak intensity ratio of the 015 dolomite ordering and 110 reference peaks (Goldsmith and Graf, 1958; Kaczmarek et al., 2017).

Iodine, Ca, and Mg in carbonate reactants and products were measured using a Thermo Scientific iCAP triple quadrupole ICP-MS according to standard procedures (Hardisty et al., 2017; Lu et al., 2020; Winkelbauer et al., 2021). Samples were weighed and rinsed in 18.2 M $\Omega$ .cm resistivity ultrapure water and dissolved in a 3 % nitric acid solution. Once fully dissolved, samples were diluted to approximately 50 ppm Ca in a 0.5 % tertiary amine solution (Inorganic Ventures uNS-2B). Dissolved, diluted samples were immediately measured to avoid loss of volatile iodine. Ca, I, and Mg were each measured in both single-quadrupole and triplequadrupole modes. Inorganic Ventures ICP-MS standards (Cs, In, Sc) were added to each sample as internal standards and used to normalize the target analytes. Japanese Coral – Porites (JCp-1) was used as a reference standard to ensure that its I/Ca value fell within the known range for the standard throughout the analysis (Lu et al., 2020). JCp-1 and a calibration standard were also monitored throughout a run as drift monitors. In instances where drift was indicated, data were corrected using the slope of the drift monitors over the course of the run.

Considering that the measured I/(Ca + Mg) represents a bulk value and that many of our samples contain various amounts of

aragonite reactant in addition to products, %product (%LMC + % HMC + %VHMC + %dolomite), which was determined via XRD, was used to calculate  $I/(Ca + Mg)_{products}$ . This procedure accounts for the presence of the reactant, which, in all experimental Series except A, contain no iodine. For Series A,  $I/(Ca + Mg)_{products}$  was calculated using the weighted average method by considering %aragonite reactant, I/Ca in aragonite reactant, %product, and measured I/(Ca + Mg). Hereafter,  $I/(Ca + Mg)_{products}$  will be used to refer to the measured I/(Ca + Mg) corrected for the presence of reactants whereas  $I/(Ca + Mg)_{dolomite}$  will be used to refer to I/(Ca + Mg) corrected for the presence of reactants in samples with > 90 % dolomite. For samples containing more than one Ca-Mg-CO<sub>3</sub> product, the average MgCO<sub>3</sub> (mol%) was calculated using the MgCO<sub>3</sub> of the individual phases and their relative abundances. The average MgCO<sub>3</sub> values are shown in Fig. 6.

#### 2.3. Trace element geochemistry

Before presenting the results, a brief overview of partition coefficients is provided. Equilibrium partitioning of an element between an aqueous solution and a mineral is described by Berthelot-Nernst distribution law (Berthelot, 1872; Nernst, 1891; McIntire, 1963):

$$K = \frac{a_{\chi}^{S}}{a_{\nu}^{L}} \tag{5}$$

Where K is the thermodynamic constant, a is activity, x is the element of interest, S refers to the solid phase, and L refers to the liquid phase. Using this relationship requires knowing the activities and achieving thermodynamic equilibrium between the two phases. Solid phase activities are often unknown and true thermodynamic equilibrium is rarely, if ever, attained under laboratory conditions (Morse and Bender, 1990). Accordingly, a widely used alternative to a thermodynamic distribution coefficient is a non-thermodynamic partition coefficient (exchange coefficient of Beattie et al., 1993) that utilizes the concept of trace and carrier components (Henderson and Kracek, 1927):

$$D = \frac{(Tr/Cr)_{S}}{(Tr/Cr)_{L}} \tag{6}$$

Where D is the partition coefficient (also referred to as distribution coefficient), Tr refers to the trace component, and Cr to the carrier component. One practical issue with the concept of carrier and trace components is that the chemical species of the element incorporated into the mineral as well as the carrier component with which it substitutes are often unknown *a priori*. Additionally, if one uses only Ca as a carrier for a given trace element in dolomite, the partition coefficient in dolomite will be inconsistent with that in calcite because one mole of a perfectly stoichiometric dolomite has half a mole of Ca compared to calcite, with the other half being Mg. To avoid the discrepancy in partition coefficients between calcite and dolomite and to be consistent with the iodine proxy convention, which divides I by the summation of Ca and Mg, we define the partition coefficient of iodine in dolomite as follows:

$$D_{\text{iodine}} = \frac{(I/(Ca + Mg))_{\text{dolomite}}}{(I/(Ca + Mg))_{\text{solution}}}$$
(7)

#### 3. Results

#### 3.1. The dolomitization reaction

Experimental data are presented in Supplemental Table S1. A typical dolomitization reaction curve is shown for Series C-3 in

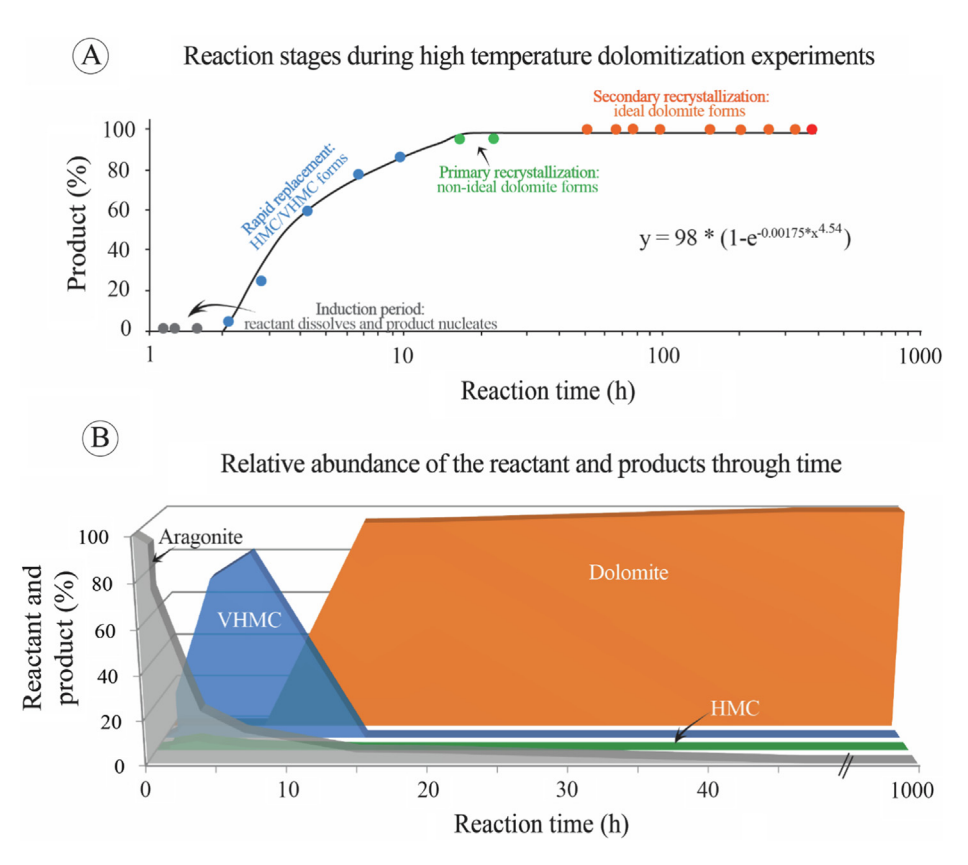


Fig. 2. (A) Cross plot between reaction time and experimental products for Series C-3 showing reaction progress and stages (experimental details are shown in Table 1). Products include low-Mg calcite, high-Mg calcite, very high-Mg calcite (i.e., protodolomite), and dolomite. A reaction curve is fitted to the data using Avrami equation (Eq. (8)). The data and the fitted curve exhibit an S-shape where initially no products form for a period of time, followed by a rapid increase In the abundance of products, followed by a decline in the growth rate as % products approaches ~ 90 %. The figure displays the four reaction stages typically observed in replacement dolomitization experiments (names are modified after Kaczmarek and Sibley, 2014). (B) the relative abundance of the reactant and products determined using XRD for Series C-3 through reaction time.

Fig. 2. This curve is fitted to the data using a modified version of the Avrami equation (Avrami, 1939):

$$y = A(1 - e^{-kx^n}) \tag{8}$$

where y is product abundance (%), x is reaction time (h), and A, k, and n are constants, which for the curve shown in Fig. 2, are 98, 0.00175, and 4.54, respectively. The constant n is related to nucleation and growth processes, k is the Avrami kinetic constant (Avrami, 1939), and A is a scaling factor to convert y values to percent. The curve is fitted to the reaction data by iteratively minimizing the difference between y values calculated from Eq. (8) and the empirical data by changing A, K, and n, ensuring that A < 100.

The relative abundances of the reactant and products are plotted as a function of time in Fig. 2B, using Series C-3 as an example. Data presented in Fig. 2A show that no products form for a certain period of time (i.e., induction period) after the onset of experiments (e.g., Kaczmarek and Sibley, 2014), followed by relatively fast increase in percent product that decelerates as percent product approaches  $\sim 90\%$  (Fig. 2). The experimental products include LMC  $(MgCO_3 < 4 mol\%)$ , HMC  $(4 mol\% < MgCO_3 < 20 mol\%)$ , VHMC (MgCO<sub>3</sub> > 20 mol%), and dolomite. As the reaction progresses, transient metastable phases are consumed at the expense of dolomite. Dolomite stoichiometry (mol% MgCO<sub>3</sub>) and cation ordering increase with reaction time (Fig. 2A and 3). The overall dolomitization reaction rate (% product/reaction time) correlates positively with temperature, and negatively with solution [KIO<sub>3</sub>] (Supplemental table S1). For example, after 8 h, Series C-1 (KIO<sub>3</sub> =  $0.2 \mu$ M) and C-2 (KIO<sub>3</sub> = 0.8  $\mu$ M) are characterized by > 40 % dolomite whereas Series C-5 (KIO<sub>3</sub> = 1000  $\mu$ M) and C-6 (KIO<sub>3</sub> = 10000  $\mu$ M) exhibit 0 % dolomite (Supplemental Table S1).

While all experiments are characterized by a decrease in aragonite abundance and an increase in dolomite abundance with time. the occurrence and abundance of the intermediate Ca-Mg-CO<sub>3</sub> phases (LMC, HMC, and VHMC) is highly variable. LMC is consistently the least abundant intermediate phase, occurring only in Series A, C-2, and D-1, with a maximum abundance of 11 % in Series C-2. HMC is identified in all Series except C-6. HMC reached its highest abundance of 18 % in Series C-5. VHMC occurs in all Series with an abundance that reaches as high as 92 %, consistent with previous work (e.g., Kaczmarek and Sibley, 2014). Ca-Mg-CO<sub>3</sub> phases do coexist but LMC and HMC are most pronounced early in the reaction before the aragonite reactant has been fully consumed. LMC and HMC abundances decrease with the increase of VHMC abundance. In all experiments, the appearance of VHMC precedes dolomite, and the two phases may coexist, but their abundances are generally inversely proportional. VHMC typically contains between 33 and 38 mol% MgCO3 and lacks evidence for cation ordering. This phase has also been called protodolomite (Graf and Goldsmith, 1956), pseudodolomite (Gaines, 1977), VHMC (Sibley et al., 1994), and disordered dolomite (e.g., Zhang et al., 2010). In the present study, this phase will be referred to as VHMC and is assumed to be the disordered precursor for stoichiometric. ordered dolomite. For a detailed discussion of dolomite-related terminology, the reader is referred to Gregg et al. (2015).

For samples with > 90 % dolomite, there is a positive correlation between reaction time and each of dolomite stoichiometry and cation ordering, as shown in Fig. 3A and 3B. Stoichiometry and cation ordering correlate with each other (Fig. 3C). While there is a general increase in stoichiometry and cation ordering with reaction time for the compiled data, there is some scatter. The

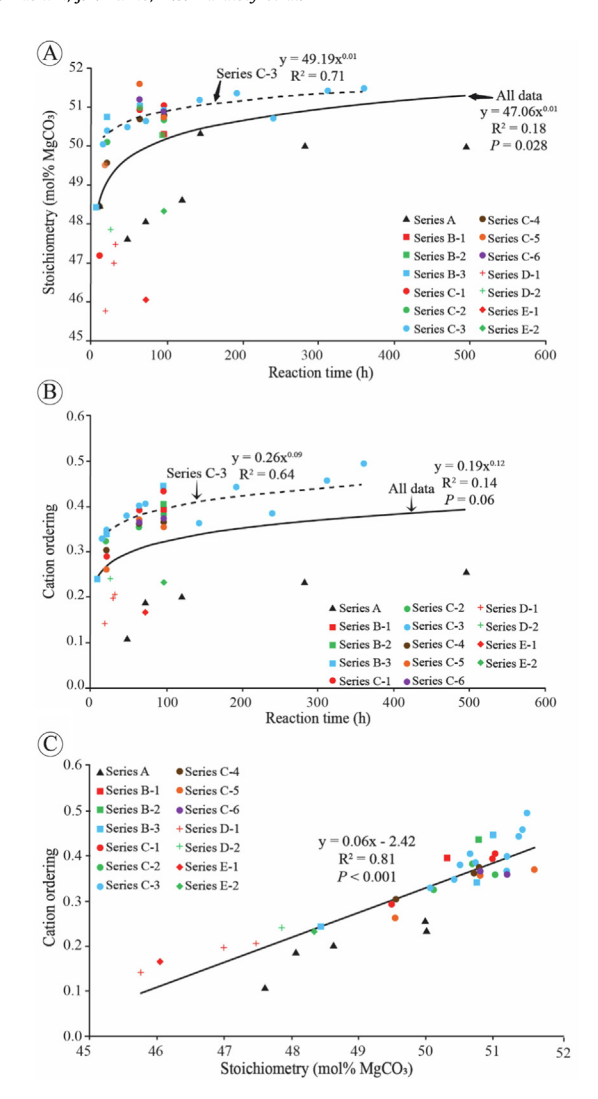


**Fig. 3.** Cross plots between dolomite stoichiometry and reaction time (A), dolomite cation ordering and reaction time (B), and stoichiometry and cation ordering (C) for samples with 90% dolomite from all Series. It can be observed that experiments that used aragonite sediments as reactants (Series A) as well as experiments conducted at temperatures lower than 200% (Series D and E) produced dolomites with lower stoichiometry and cation ordering values. All experimental conditions are presented in Table 1.

relationships are stronger ( $R^2$  is higher) for data from individual Series as demonstrated in Fig. 3.

## 3.2. Loss of iodine from carbonate sediments

Experiments in Series A, whereby aragonite-dominated sediments with an average I/(Ca + Mg) ratio of  $8.7 \pm 0.19 \ \mu mol/mol$  were dolomitized in iodine-free solution, show that  $I/(Ca + Mg)_{products}$  decreases rapidly with reaction time and reaches zero after 72 h (Fig. 4). Only the first two samples, which are characterized by 22 % and 96 % dolomite, respectively exhibit a nonzero I/(Ca + Mg) ratio in the bulk solids.

## 3.3. Iodine content of the Ca-Mg-CO<sub>3</sub> products

All experiments conducted using a solution containing KIO<sub>3</sub> (Series C, D, and E)—i.e., IO<sub>3</sub> only— produce Ca-Mg-CO<sub>3</sub> products containing iodine (Fig. 5). In contrast, experiments conducted using KI solutions (Series B)—i.e., I<sup>-</sup> only—result in products containing no iodine (Fig. 5). For the KIO<sub>3</sub> experiments, the

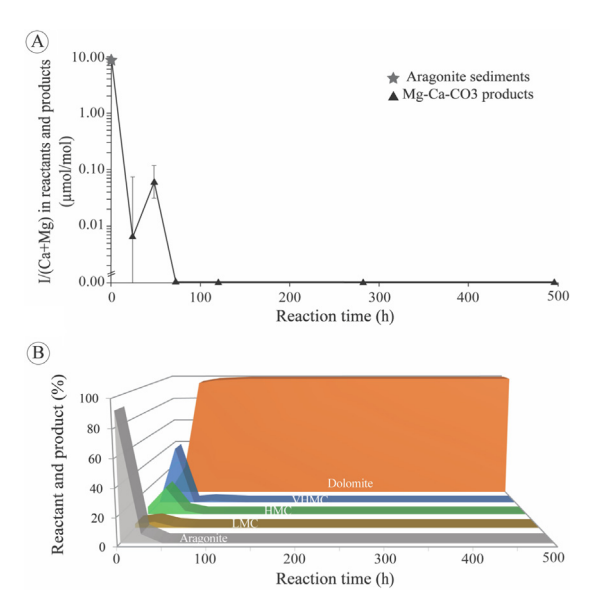


**Fig. 4.** (A) I/(Ca + Mg) ratios in the reactant (the star) and products (triangles) over time for Series A. The star represents I/(Ca + Mg) in the aragonite sediments used as a reactant for Series A experiments. Before the beginning of the experiments (i.e., time = 0 h), the reactant contains 8.7  $\mu$ mol/mol I/(Ca + Mg). As the aragonite sediments get dolomitized, the I/(Ca + Mg) in the products (triangles) decreases rapidly followed by its complete loss from the products during dolomitization. (B) The relative abundance of the reactant and products for Series A through reaction time

I/(Ca + Mg)<sub>products</sub> correlates strongly with the I/(Ca + Mg)<sub>solution</sub> (Fig. 5). However, it is important to note that the solutions used in our experiments span a wide range of I/(Ca + Mg) values that far exceed the range of seawater. When only experiments that span the natural range of I/(Ca + Mg)<sub>solution</sub> are examined (i.e., excluding Series C-5 and C-6), the  $R^2$  of the correlation between I/(Ca + Mg)<sub>products</sub> and in solution decreases slightly to 0.79 but the *P*-value remains < 0.001 suggesting a statistically significant correlation (Fig. 5).

All experiments conducted in KIO<sub>3</sub> solutions exhibit a general decrease in I/(Ca + Mg)<sub>products</sub> with reaction time and with MgCO<sub>3</sub> of the products. This is shown for Series C in Fig. 6. The only exception is Series C-1, which exhibits an increase in I/(Ca + Mg)<sub>products</sub> followed by a decrease to zero (Fig. 6). It is not exactly clear why I/(Ca + Mg)<sub>products</sub> in this series increases with time and with MgCO<sub>3</sub> before it decreases again but one explanation is related to the proportions of the products in this series. Specifically, experiment C-1-2, which contains higher I/(Ca + Mg)<sub>products</sub> than the preceding and following experiments in the same series, also contains higher percentages of VHMC (28 %) which likely incorporates higher amounts of iodine (Supplemental Table S1). One argument against this explanation is that the preceding experiment (C-1-1) contains even higher proportion of VHMC but lower I/(Ca + Mg)<sub>products</sub>. It is therefore likely that the abnormally high I/(Ca + Mg)<sub>products</sub> in experiment C-1-2 is related to uncertainties in either iodine measurement or XRD-derived mineralogical estimates.

Series C-3 includes longer-term experiments aimed at evaluating the effect of dolomite stoichiometry and cation ordering changes during recrystallization on  $I/(Ca + Mg)_{dolomite}$ . Results from Series C-3 show that  $I/(Ca + Mg)_{dolomite}$  decreases linearly with dolomite stoichiometry (mol% MgCO<sub>3</sub>) and cation ordering (Fig. 7).

Experiments conducted using similar [KIO<sub>3</sub>] in the solution but different temperatures show that there is no statistically significant correlation between temperature and  $I/(Ca + Mg)_{dolomite}$  of the first sample with > 90 % dolomite (Fig. 8A). Moreover, dolomites from experiments shown in Fig. 8A are characterized by dif-

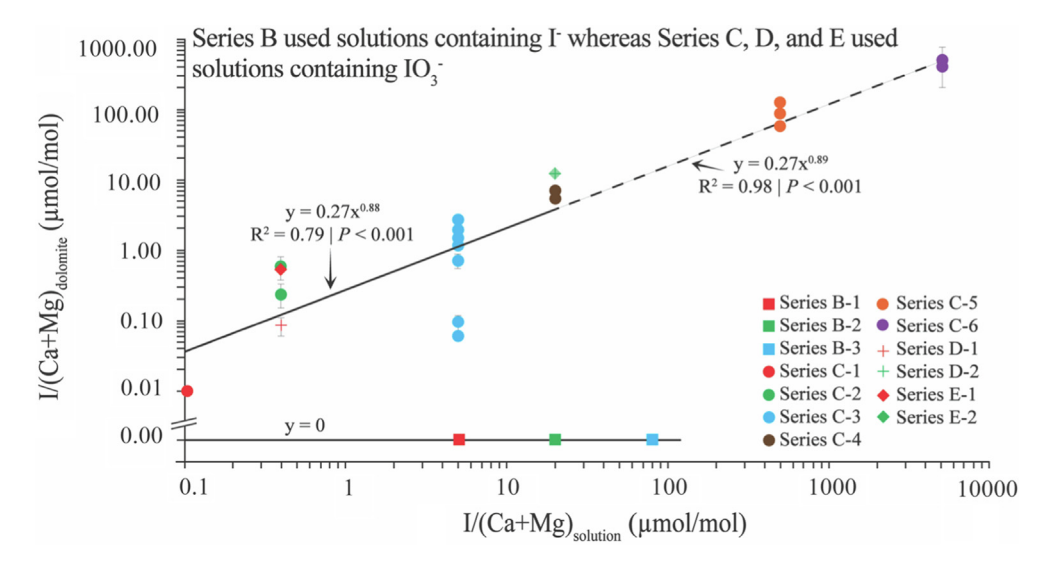
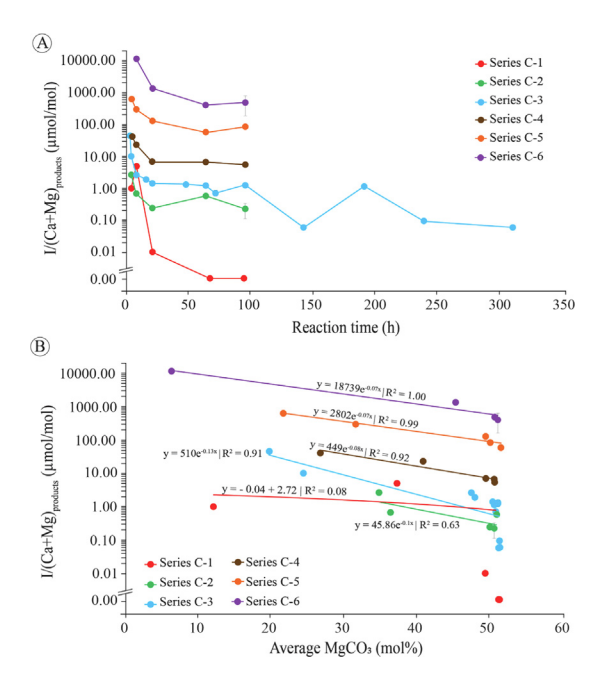


Fig. 5. Plot between I/(Ca + Mg) ratios in the solution and in dolomite for samples with > 90 % dolomite from all Series except A. All Series plotted here used an aragonite reactant with zero iodine. Experiments conducted in solutions containing  $KIO_3$  solutions (all Series except B) resulted in dolomite with non-zero I/(Ca + Mg) values whereas experiments conducted in KI solutions (Series B) yield dolomites with I/(Ca + Mg) = zero, I/(Ca + Mg) =



**Fig. 6.** Cross plot between  $I/(Ca + Mg)_{products}$  and each of reaction time (A) and average  $MgCO_3$  of the products (B) for all samples from Series C. Note that an exponential function is fitted to data from all Series except C-1, where a linear function is fitted instead, because one sample form Series C-1 has a zero I/(Ca + Mg).

ferent cation ordering values (Fig. 8B). This is important because there is a statistically significant linear correlation between cation ordering and I/(Ca + Mg)<sub>dolomite</sub> for samples from experiments conducted at different temperatures (Fig. 8B).

#### 4. Discussion

The following discussion focuses on the following themes: 1) the replacement dolomitization reaction; 2) the iodine species (iodate or iodide) incorporated into dolomite; 3) the effect of dolomitization on the iodine content in carbonate sediments; 4) the

controls on iodine incorporation into dolomite; 5) iodate partition coefficient; and 6) the implications of the experimental findings to the iodine paleoredox proxy, Precambrian dolomitization, and the shallow ocean of the Proterozoic.

#### 4.1. The stepwise dolomitization model

The data presented here are generally consistent with previous findings that experimental dolomitization of CaCO<sub>3</sub> proceeds via a series of replacement reactions whereby each successive product is more stable than its precursor (e.g., Katz and Matthews, 1977; Sibley et al., 1987; Kaczmarek and Sibley, 2007, 2011, 2014; Kaczmarek and Thornton, 2017; Kell-Duivestein et al., 2019; Teoh et al., 2022). The dolomitization reaction starts with an induction period (Sibley et al., 1987; Kaczmarek and Sibley, 2014) during which the aragonite reactant begins to dissolve, and nucleation of VHMC ensues, but no significant growth of products occurs (Fig. 2). The induction period is followed by a rapid replacement period (Kaczmarek and Sibley, 2014) characterized by a relatively fast growth of VHMC often accompanied by the growth of lesser amount of HMC and rarely LMC (Fig. 2). The replacement period is followed by a stage of primary recrystallization (Kaczmarek and Sibley, 2014) where VHMC dissolves and a poorly ordered dolomite precipitates as evidenced by an increase in cation ordering and stoichiometry. The final reaction stage is secondary recrystallization (Kaczmarek and Sibley, 2014), during which the stoichiometric but poorly ordered dolomite recrystallizes to wellordered dolomite as evidenced by the observation that cation ordering continues to increase despite the no changes in the stoichiometry (Fig. 2).

#### 4.2. Determining the iodine species incorporated into dolomite

Experiments conducted using a  $KIO_3$  solution, representing oxidized iodine ( $IO_3$ ), yields products containing various amounts of I/(Ca + Mg) whereas those conducted using a KI solution, representing reducing iodine ( $I^-$ ), resulted in products with no iodine (Fig. 5). These results suggest that the iodine species incorporated into dolomite and other  $Ca-Mg-CO_3$  phases that formed in our experiments is iodate, which validates the iodine redox proxy in

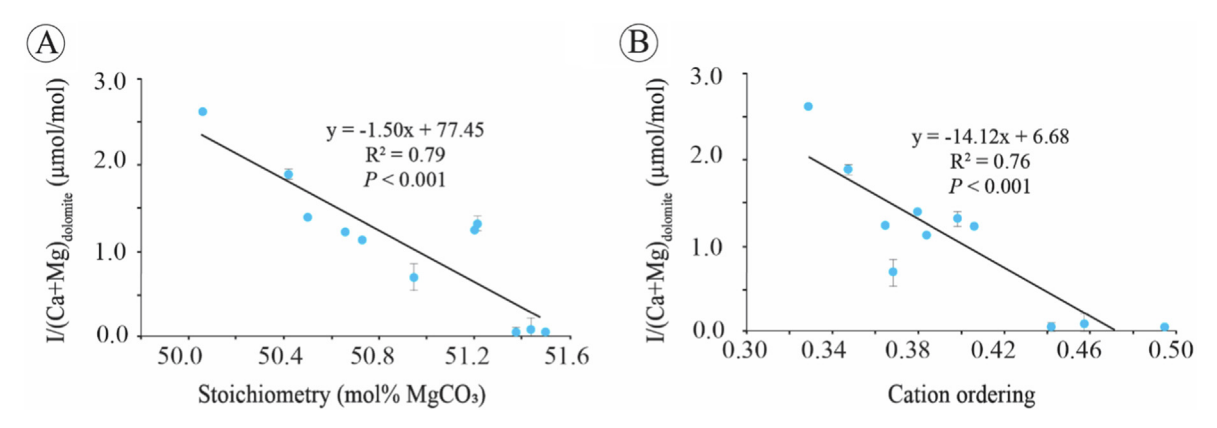


Fig. 7. Cross plot between I/(Ca + Mg) ratios and each of dolomite stoichiometry (A) and cation ordering (B) for samples with > 90 % dolomite from Series C-3. In both cases, there is a statistically significant negative correlation.

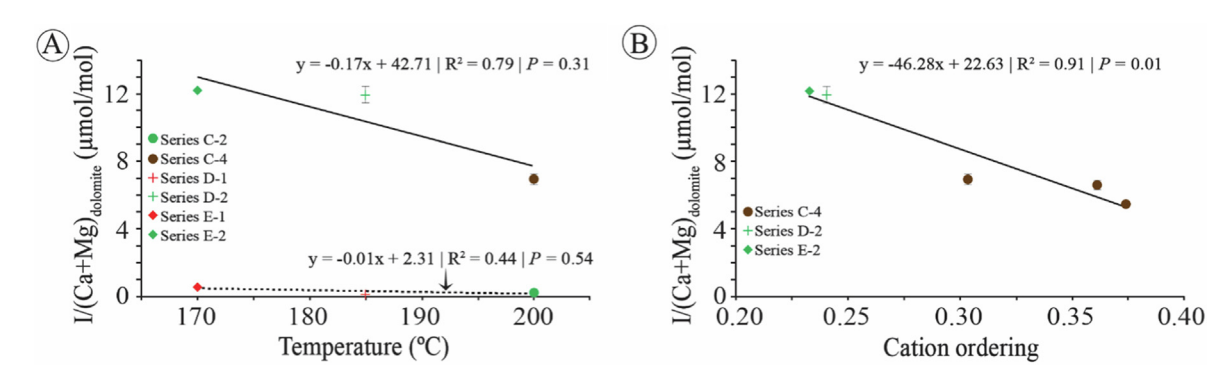


Fig. 8. (A) cross plot between I/(Ca + Mg) ratios in dolomite and reaction temperature for the first sample with > 90 % dolomite from each Series. Series C-2, D-1, and E-1 were conducted using solution I/(Ca + Mg) ratio of 0.4  $\mu$ mol/mol whereas Series C-4, D-2, and E-2 used solution I/(Ca + Mg) ratio of 20  $\mu$ mol/mol. While the correlations between I/(Ca + Mg) in dolomite and temperature are strong, they are statistically insignificant based on P values (B) cross plot showing a strong and statistically significant correlation between I/(Ca + Mg) ratios in dolomite and cation ordering for all samples with > 90 % dolomite from Series C-4, D-2, and E-2. It should be noted that in (A) we plot only the first sample with > 90 % dolomite from each Series in order to compare samples with dolomites that have similar stoichiometry and cation ordering. In (B) we plot all samples from each series in order to demonstrate the relationship between I/(Ca + Mg) and cation ordering given that dolomite ordering increases with reaction time.

dolomite, and implies that the presence of iodine in natural dolomites (i.e., non-zero I/(Ca + Mg)) likely reflects iodate, and thus oxygen, in the dolomitizing fluids.

An outstanding question is why iodate  $(IO_3^-)$  is incorporated into dolomite, but iodide  $(I^-)$  is not? Insights relevant to this question can be derived from studies of iodine incorporation in calcite. Lu et al. (2010) hypothesized that  $IO_3^-$  substitutes for  $CO_3^{2-}$  in calcite based on the similarities in the Ca–O bond length in the naturally occurring mineral lautarite  $(Ca(IO_3)_2)$  and calcite  $(CaCO_3)$  as well as the I–O bond length in  $IO_3^-$  and the C–O in  $CO_3^{2-}$  (Table 2). Based on

**Table 2**Bond lengths and ionic radii of the bonds and ions discussed in the text.

Bond	Bond length (Å)
Ca-O in Ca(IO <sub>3</sub> ) <sub>2</sub> (lautarite)	2.5
Ca-O in CaCO <sub>3</sub> (calcite)	2.4
I-O in IO <sub>3</sub>	1.8
C—O in CO <sub>3</sub> <sup>2-</sup>	1.3
Ion	Ionic radius (Å)
K <sup>+</sup>	1.38
Na <sup>+</sup>	1.02
Ca <sup>2+</sup>	1.00
H <sup>+</sup>	1.54
$Mg^{2+}$	0.72
IO <sub>3</sub>	1.22
CO <sub>3</sub> <sup>2-</sup>	1.78

molecular dynamics simulations and extended X-ray absorption fine structure spectroscopy data, Kerisit et al. (2018) suggested that  $IO_3^-$  is incorporated into calcite by substituting with  $CO_3^{2-}$ and the charge compensation is achieved by the substitution of Na<sup>+</sup> or H<sup>+</sup> with Ca<sup>2+</sup>. It is not unreasonable to assume that this model also applies to dolomite. We propose, however, that H<sup>+</sup> balances the charge by substituting with Ca<sup>2+</sup> because our solutions were devoid of Na<sup>+</sup>. If H<sup>+</sup> does indeed participate in this substitution, solution pH should strongly impact the incorporation of IO<sub>3</sub> in carbonate minerals (Kerisit et al., 2018), and thus may represent another control on iodine content in carbonate minerals. Similarly, Li incorporation into calcite has been suggested to be pH dependent as it requires charge balance suggested to be achieved through its incorporation as LiHCO<sub>3</sub> (Sevedali et al., 2021). Another potential candidate to compensate the charge imbalance resulting from the substitution of  $IO_3^-$  with  $CO_3^{2-}$  is  $K^+$ , which was present in all our experimental solutions. Although K<sup>+</sup> has a larger ionic radius than both Na<sup>+</sup> and Ca<sup>2+</sup> (Table 2), K<sup>+</sup> and Na<sup>+</sup> have been shown to exhibit a similar mode of incorporation into calcite (Ishikawa and Ichikuni, 1984; Hashim and Kaczmarek, 2020), supporting the proposition that K<sup>+</sup> may balance the charge in these experiments by substituting with Ca<sup>2+</sup> or Mg<sup>2+</sup>. Further work is needed to determine whether H<sup>+</sup> or K<sup>+</sup> balances the charge that results from the substitution of  $IO_3^-$  with  $CO_3^{2-}$ . In contrast to  $IO_3^-$ , I is not incorporated into dolomite (Fig. 5) likely because it is incompatible with the dolomite crystal structure (Lu et al., 2010).

#### 4.3. Loss of iodine from carbonate sediments

We tested for the impacts of dolomitization of iodate-containing primary aragonite precipitated from an oxic water column. Specifically, results from Series A in which iodine-containing aragonite sediments were dolomitized in iodine-free solution, show that only a small proportion of the (I/(Ca + Mg) values in the sediment reactant was retained by Ca-Mg-CO<sub>3</sub> products, followed by its complete exclusion in the dolomite as the reaction progresses (Fig. 4). This result is consistent with the expectation that dolomite formed in anoxic—and thus iodate-free—pore fluids will not be rock buffered and will have lower I/(Ca + Mg) ratios compared to primary sediments formed in oxic conditions. These experiments reinforce observations of low I/(Ca + Mg) in diagenetic dolomite from the Bahama Bank (Hardisty et al., 2017) and low I/(Ca + Mg) in some ancient dolomite samples (e.g., Loope et al., 2013).

Since dolomitization in Series A took place in iodine-free solutions, the only source of iodine is the reactant, which must release its iodine into the solution during dissolution. Given that the iodine content of the aragonite sediments is known, [IO<sub>3</sub>] in the solution from which the Ca-Mg-CO<sub>3</sub> products precipitated can be calculated. The aragonite sediments contain I/(Ca + Mg) of 8.7 μmol/mol, or 7.53 mg of iodine per kg aragonite. After the dissolution of 0.2 g of aragonite in 15 mL of solution, [I-] in the solution would be 0.8  $\mu$ M, which is equal to the [IO<sub>3</sub>] used in Series C-2 (Table 1). The results from Series A and C-2 are, therefore, directly comparable because products should have presumably formed from solutions with identical iodine concentrations and thus would be expected to contain similar I/(Ca + Mg) ratios. Surprisingly, Ca-Mg-CO<sub>3</sub> products from Series A were lower in I/(Ca + Mg) by at least an order of magnitude compared to those from Series C-2 (Supplemental Table S1). We consider the following three hypotheses to explain this observation: iodide release, impurities, and reaction rate.

First, at least some of the iodine in the aragonite sediment used in Series A might be in the form of iodide. While iodate has been demonstrated as the only iodine species incorporated into calcite (Lu et al., 2010; Zhou et al., 2014) and now dolomite, similar experiments have not been performed to confirm this observation for aragonite. If iodide can be incorporated in aragonite, the dissolution of aragonite would release into the solution both iodate and iodide with a total concentration of 0.8  $\mu$ M but [IO $_3$ ] of < 0.8  $\mu$ M. Based on the understanding that only iodate is incorporated into dolomite (Section 4.2), it is assumed that dolomite from Series A would incorporate less I/(Ca + Mg) than that in Series C-2 where [IO $_3$ ] = 0.8  $\mu$ M.

Second, the difference in the I/(Ca + Mg) between Series A and C-2 may be explained by impurities (Sr, Mg, Na, K, organic matter, etc.) in Series A reactants, which upon dissolution, would be released into the solution. Although we did not determine the elemental composition of reactants, aragonite sediments are known to host a wide variety of trace elements (e.g., Swart, 2015; Smrzka et al., 2019; Li et al., 2019) that could react with iodate and form aqueous complexes, which decreases iodate activity in the solution.

A third explanation for why Series A and C-2 products contain different amounts of I/(Ca + Mg) despite presumably similar iodine concentrations in the solutions could be related to the difference in the overall reaction rate between the two series (Supplemental Table S1). That is, the dolomite in Series A incorporated less iodine possibly because it formed at a slower rate compared to the dolomite in Series C-2. While the limited number of individual experiments conducted in each of Series A and C-2 does not allow us to detect clear differences in reaction rates between the two series, the data suggest that the overall reaction rate in Series A was

slower compared to Series C-2. For example, 93 % product was achieved after 24 h of reaction time in Series A compared to 8 h in Series C-2 (Supplemental Table S1). Reaction rate has been shown to increase trace element incorporation into calcite (e.g., Mavromatis et al., 2013) though a similar effect in dolomite has not yet been observed. While we did not test the effect of reaction rate on iodine incorporation, we discuss this possibility further in Section 4.4.2.

Despite the difference between Series A and C-2, the observation that dolomite in Series A retains only a small proportion of the initial iodine from the reactant is expected given the only source of iodine is the reactant and because of the high fluid:solid ratio used in the experiments (i.e., fluid-buffered conditions). Under such conditions, the dissolution of a small mass of aragonite into a large volume of an initially iodine-free solution leads to a low iodine concentration in the solution from which the various Ca-Mg-CO<sub>3</sub> phases precipitate.

#### 4.4. Controls on iodine incorporation into dolomite

Experiments conducted using solutions with various  $KIO_3$  concentrations show that there is a strong positive correlation between  $I/(Ca + Mg)_{dolomite}$  and  $I/(Ca + Mg)_{solution}$  (Fig. 5). This observation suggests that iodate content in dolomite is dictated by the iodate concentration of the solution and implies that a partition coefficient for iodate in dolomite can be derived (discussed in Section 4.5). Yet, experiments that used similar  $I/(Ca + Mg)_{solution}$  yielded dolomites with variable I/(Ca + Mg) values (Figs. 5 and 6), suggesting that additional factors other than  $I/(Ca + Mg)_{solution}$  must exert some control on  $I/(Ca + Mg)_{dolomite}$ . We discuss below some of the tested variables that influence iodine incorporation into dolomite before deriving a partition coefficient for iodate.

# 4.4.1. Effects of $MgCO_3$ content, dolomite stoichiometry, and cation ordering

The observation that the amount of I/(Ca + Mg)<sub>products</sub> decreases with increasing reaction time (Fig. 6A) could indicate active iodate reduction during the experiments. The iodate concentrations of the evolving experimental solutions were not measured, thus limiting constraints on this hypothesis. However, while we cannot rule out minor iodate reduction, several other observations argue against significant, if any, iodate reduction occurring in our experiments. Fig. 6 shows that  $I/(Ca + Mg)_{products}$  in Series 6 decreases from  $\sim$  10,000 to < 1,000  $\mu$ mol/mol with reaction progress but that experiments with initial I/(Ca + Mg)<sub>products</sub> of < 100 μmol/mol (Series 2, 3, and 4) decreases to non-zero values. Given that these experiments were conducted under identical conditions except for dissolved [IO3], we would expect similar magnitudes of decrease in I/(Ca + Mg)<sub>products</sub> if active [IO<sub>3</sub>] reduction was the main control, but this was not observed. Compounding this is the observation that after the initial period of decrease, I/(Ca + Mg)<sub>products</sub> remains nearly constant, and in some cases, even increases with reaction time (Fig. 6A). Interestingly, the same period of reaction time during which I/(Ca + Mg)<sub>products</sub> decreases most significantly (Fig. 6A) is when dolomite stoichiometry and cation ordering change the most (Fig. 3A and 3B). Furthermore, similar trends (i.e., continuous decrease in trace element concentration with reaction time after dolomite formation) to those observed here for iodate have also been observed with other trace elements that are not redox sensitive (e.g., Katz and Matthews, 1977; Malone et al., 1996). Collectively, these observations indicate that the decrease in I/(Ca + Mg) products with time is unlikely to be related to redox reactions. Alternatively, we propose that the observed decrease in I/(Ca + Mg)<sub>products</sub> with reaction time (Fig. 6A) is related to dolomite chemical and structural characteristics.

The correlation between I/(Ca + Mg)<sub>products</sub> with the MgCO<sub>3</sub> in the bulk solids (Fig. 6B) suggests that each one of the Ca-Mg-CO<sub>3</sub> phases that form in our experiments (LMC, HMC, VHMC, dolomite) incorporates a different amount of I/(Ca + Mg) and thus has its own D. This means that the amount of I/(Ca + Mg) in the solid phases is a function of their chemical composition (i.e., MgCO<sub>3</sub>), which is consistent with previous work on the partitioning of trace elements between the aqueous solution and calcite (e.g., Mucci and Morse, 1983; Ohde and Kitano, 1984). Mucci and Morse (1983) demonstrated that  $D_{Mg}$  and  $D_{Sr}$  are functions of calcite MgCO $_3$  content by showing that the amount of Sr incorporated into calcite increases with the increase of calcite MgCO<sub>3</sub>. They attributed this phenomenon to the lattice distortion created by substitution of the smaller Mg with Ca, which increases the number of sites available for Sr, and thus more Sr can be incorporated. This argument cannot be directly applied to explain our observations for several reasons. First, we observe an opposite trend (decreasing I/(Ca + Mg) with increasing MgCO<sub>3</sub>) to the trend observed by Mucci and Morse (1983). Second, fundamental differences exist between  $IO_3^-$  which is hypothesized to substitute with  $CO_3^{2-}$  and requires a charge balance (Section 4.2), and Sr<sup>2+</sup> which is proposed to substitute primarily with Ca<sup>2+</sup>. We offer the following hypothesis to explain the decrease in I/(Ca + Mg) values with the increase of the MgCO<sub>3</sub> of the solid phases.

The substitution of  $IO_3^-$  with  $CO_3^2^-$  causes a charge disparity that needs to be balanced (Kerisit et al., 2018) and, in our experiments, H<sup>+</sup> and K<sup>+</sup> are the most likely candidates to balance the charge by substituting with  $Ca^{2+}$  or  $Mg^{2+}$  (Section 4.2). While H<sup>+</sup> and K<sup>+</sup> are larger than both  $Ca^{2+}$  and  $Mg^{2+}$ ,  $IO_3^-$  is smaller than  $CO_3^{2-}$  (Table 2), and thus the substitution of  $IO_3^-$  with  $CO_3^{2-}$  should create an extra space to accommodate large ions such as H<sup>+</sup> and K<sup>+</sup>. In fact, the difference in ionic radius between  $IO_3^-$  and  $CO_3^{2-}$  (0.56 Å) is almost identical to the difference between H<sup>+</sup> and  $Ca^{2+}$  (0.54 Å). Importantly, because both H<sup>+</sup> and K<sup>+</sup> are closer in size to  $Ca^{2+}$  than to  $Ca^{2+}$ , they are more likely to substitute with  $Ca^{2+}$  than with  $Ca^{2+}$ , they are more likely to substitute with  $Ca^{2+}$  than with  $Ca^{2+}$  and  $Ca^{2+}$  is expected to accommodate more iodine than a phase with a higher mol%  $Ca^{2+}$  MgCO<sub>3</sub>, which may explain the decrease of  $Ca^{2+}$  Mg) with the increase of mol% MgCO<sub>3</sub> (Fig. 6).

The same argument may explain the decrease in I/(Ca + Mg) ratios with the increase of MgCO<sub>3</sub> in the Ca-Mg-CO<sub>3</sub> phases and with the increase of dolomite stoichiometry (Figs. 6 and 7A). However, because the increase in dolomite stoichiometry is accompanied by an increase in cation ordering (Fig. 3C), it is possible that the decrease in I/(Ca + Mg) ratios is related to both cation ordering and stoichiometry (Fig. 7). If true, what could explain the influence of cation ordering on I/(Ca + Mg)<sub>dolomite</sub>? When cation ordering increases, the dolomite crystal structure becomes less distorted (Reeder and Wenk, 1983; Land, 1985). Reeder and Wenk (1983) observed increases in unit cell parameter c and unit cell volume and changes in interatomic distances as a result of thermally induced disordering. Such changes could modify how able the crystal lattice is to accommodate "foreign" compounds like iodate, which may explain the observed decrease in I/(Ca + Mg) ratios with increasing ordering (Fig. 7B). It is worth mentioning that our observation that I/(Ca + Mg) decreases with the increase of dolomite stoichiometry and cation ordering is consistent with previous studies that investigated trace elements in dolomite in experimental (e.g., Katz and Mathews, 1977; Malone et al., 1996) and natural settings (e.g., Vahrenkamp and Swart, 1990; Montanez and Read, 1992).

## 4.4.2. Effect of temperature

Experiments conducted using solutions with the same  $[KIO_3]$  but different temperatures show that there is a slight decrease in the amount of I/(Ca + Mg) with increasing temperature for samples with > 90 % dolomite (Fig. 8A). While these data could indicate that

the amount of I/(Ca + Mg)<sub>dolomite</sub> is influenced by reaction temperature, the observed correlation is statistically insignificant based on the calculated P values (Fig. 8A). Importantly, a closer look at the dolomite samples plotted in Fig. 8A reveals that they are compositionally and structurally dissimilar. Particularly, the dolomites from the higher temperature experiments have higher cation ordering values. As discussed earlier (Section 4.4.1) and shown in Fig. 8B for the specific samples plotted in Fig. 8A, I/(Ca + Mg) ratios decrease with increasing cation ordering, suggesting that the observed relationship between I/(Ca + Mg) ratios and temperature (Fig. 8A) can be explained by the increase in cation ordering with temperature. Accordingly, the current data is inconclusive regarding whether there is a direct temperature effect on I/(Ca + Mg)<sub>dolomite</sub> within the investigated range but suggestive of an indirect effect through cation ordering. The inconclusiveness arose from our failure to capture dolomites with the exact composition and structural ordering in experiments conducted at different temperatures. This task is not trivial because reaction rate, stoichiometry, and cation ordering vary with temperature (Kaczmarek and Thornton, 2017) and both stoichiometry and cation ordering increase rapidly after the formation of dolomite (Fig. 3), making it difficult to obtain samples with similar stoichiometry and cation ordering from experiments conducted at different temperatures. Regardless, the current data can be used to qualitatively examine the relationship, or the lack thereof, between temperature and I/(Ca + Mg). If one assumes that there indeed is a relationship between I/(Ca + Mg) and temperature, it is difficult to reconcile the observation that I/(Ca + Mg) decreases with increasing temperature (Fig. 8A) with observations from previous experimental studies which indicate that increasing temperature either has no impact or increases trace element content in dolomite. For example, Katz and Matthews (1977) showed that Sr incorporation into dolomite is temperature independent over the range of 252-295 °C. Malone et al. (1996) observed a decrease in the partition coefficient of Sr (D<sub>Sr</sub>) with increasing temperature, which also increased the fractional extent of recrystallization. Importantly, Malone et al. (1996) also noted a significant decrease in D<sub>Sr</sub> with increasing recrystallization spanning a single temperature and suggested that recrystallization more significantly controls D<sub>Sr</sub> than temperature does. In other words, dolomites at higher temperature have a lower D<sub>Sr</sub> because they experienced a higher degree of recrystallization not because temperature increased Sr incorporation. Since cation ordering increases with recrystallization, the observations and interpretation of Malone et al. (1996) are similar to ours in that temperature increases recrystallization/ordering which decrease the amount of trace element incorporated into dolomite. That is, what appears to be a direct temperature control on trace element content may simply indirectly reflect an increase in cation ordering. It is also worth noting the decrease in I/(Ca + Mg)<sub>dolomite</sub> with increasing temperature is inconsistent with several previous experimental studies on the incorporation of trace elements in calcite. For example, there is overwhelming evidence that both  $D_{\text{Mg}}$  and  $D_{\text{Sr}}$  in calcite increase with temperature (Mucci, 1987; Zhang and DePaolo, 2020). Consequently, the observed decrease in I/(Ca + Mg) with increasing temperature (Fig. 8A) appears to be a mere correlation resulting from the increase of cation ordering, which decreases I/(Ca + Mg), with temperature.

A relevant aspect of this discussion is the effect of reaction rate, which is known to increase with temperature and has been demonstrated to impact the incorporation of some trace elements in calcite (Tang et al., 2008; Mavromatis et al., 2013; Gabitov et al., 2014; Alkhatib et al., 2022). For example, both  $D_{\rm Mg}$  and  $D_{\rm Sr}$  in calcite have been experimentally shown to increase with precipitation rate (e.g., Mavromatis et al., 2013; Zhang and DePaolo, 2020). If reaction rate impacts iodate incorporation into dolomite

in a similar manner, one would expect I/(Ca + Mg) to increase with increasing temperature because dolomite precipitation rate increases with temperature (Arvidson and Mackenzie, 1999). Since we observed I/(Ca + Mg) to decrease with increasing temperature (Fig. 8A), our data suggest that I/(Ca + Mg) is unlikely to be influenced by reaction rate under the current experimental conditions. This is consistent with the study of Malone et al. (1996), who observed no difference in  $D_{Sr}$  between two experimental Series despite a 4x difference in recrystallization rate.

While the apparent independence of iodate incorporation into dolomite on temperature and reaction kinetics is promising for the iodine redox proxy, this independence is only observed over a rather narrow range of conditions that differ from those under which most natural dolomite forms. It is possible that iodate is rate independent when the rate is fast but becomes dependent under slower rates. Accordingly, these ranges must be expanded to include lower temperatures and slower rates.

#### 4.5. Iodate partition coefficient in dolomite

The partition coefficient of iodate (Diodate), which relates I/(Ca + Mg) ratios in the solution and in dolomite, can be calculated using Eq (7). Fig. 9 presents the calculated D<sub>iodate</sub> values plotted against I/(Ca + Mg)<sub>solution</sub>, stoichiometry, and cation ordering. The relationship between D<sub>iodate</sub> and I/(Ca + Mg)<sub>solution</sub> is important to explore because it can provide insights into the behavior of Diodate. Specifically, the independence of D<sub>iodate</sub> on I/(Ca + Mg)<sub>solution</sub> may imply that iodate incorporation in dolomite follows a classical thermodynamic behavior whereas its dependence may reveal a kinetic influence (e.g., Mucci and Morse, 1983). Furthermore, it is important to determine whether Diodate covaries with I/(Ca + Mg)<sub>solution</sub> because [IO<sub>3</sub>], [Ca], and [Mg] are highly variable in natural waters. It is also important to evaluate the relationship between D<sub>iodate</sub>, stoichiometry, and cation ordering given that the observations presented here suggest that I/(Ca + Mg)<sub>dolomite</sub> covaries with these two mineralogical characteristics (e.g., Fig. 7).

The observation that the relationship between Diodate and I/(Ca + Mg)<sub>solution</sub> (Fig. 9A) is statistically insignificant (p-value > 0.05) suggests that iodate incorporation in dolomite is independent of I/(Ca + Mg)<sub>solution</sub> over the investigated range. This is also consistent with the small ( $< 10^{-4}$ ) slopes between D<sub>iodate</sub> and I/(Ca + Mg)<sub>solution</sub>. The slope values could be misleading, however, since the I/(Ca + Mg)<sub>solution</sub> (x-axis) range is orders of magnitude larger than the range of Diodate values (y-axis). If we exclude Series C-5 and C-6, which used I/(Ca + Mg)<sub>solution</sub> of 500 and 5000 µmol/mol respectively, the slopes become larger (-0.01 if all data is considered and -0.03 if only the first dolomite from each series is considered). While these slopes imply that there is a negative correlation between D<sub>iodate</sub> and I/(Ca + Mg)<sub>solution</sub>, the data in Fig. 9A show dolomites that are compositionally and structurally dissimilar permitting the idea that at least some of the variations in D<sub>iodate</sub> may be attributed to differences in dolomite mineralogical characteristics. Indeed, the data suggest that there are linear negative correlations between Diodate and each of stoichiometry and cation ordering (Fig. 9B and 9C), which are expected based on the observation that I/(Ca + Mg)<sub>dolomite</sub> varies with stoichiometry and cation ordering (Fig. 7). Specifically, when considering the first sample with 90 % dolomite from each series (open symbols in Fig. 9A) the data show that all dolomites have Diodate values between 0.2 and 0.6 except one sample from Series E-1 and one from Series C-6, which have higher and lower Diodate values, respectively (Fig. 9A). The E-1 sample has notably lower stoichiometry and cation ordering values whereas the C-6 sample has notably higher values (Fig. 9B and 9C). It is therefore evident that the negative correlation between Diodate and I/(Ca + Mg)solution is attributable to differences in dolomite stoichiometry and cation order-

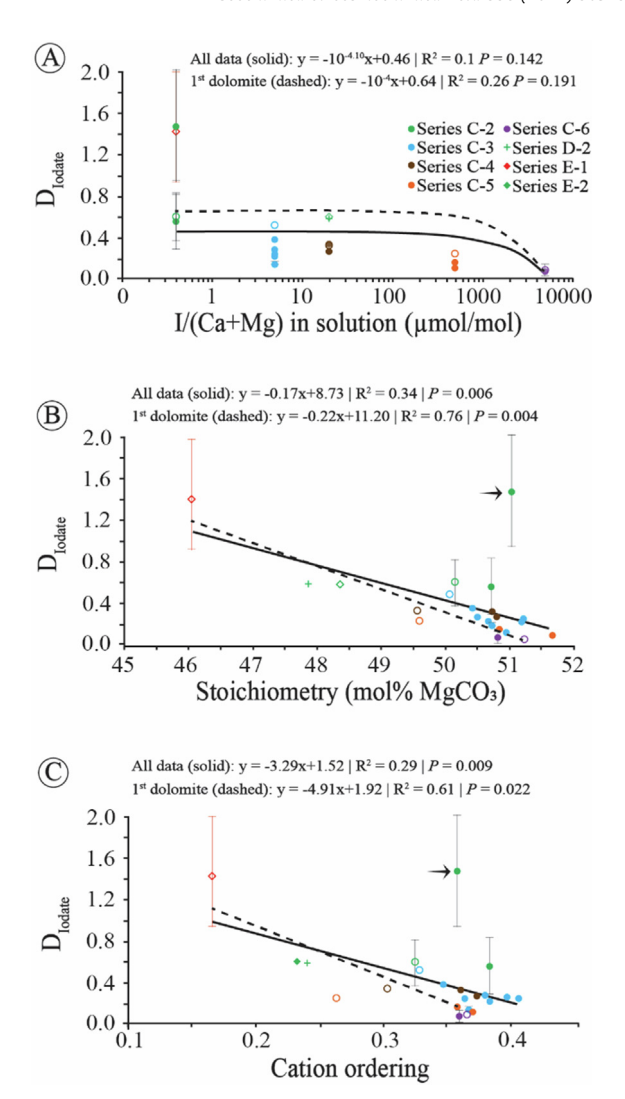


**Fig. 9.** Plots between the partition coefficient of iodate ( $D_{iodate}$ ) against each of I/(Ca + Mg) ratios in the solution (A), dolomite stoichiometry (B), and cation ordering (C). Solid symbols represent samples with > 90 % dolomite from each experimental series and solid lines are fitted through these data whereas open symbols represent the first sample with > 90 % dolomite from each experimental series and dashed lines are fitted through these data. The arrows in plots B and C mark the datapoint that has been excluded in deriving Eq. 9 (see text for details).

ing between samples, suggesting that the relationship between  $D_{iodate}$  and  $I/(Ca + Mg)_{solution}$  is less pronounced than it appears in Fig. 9A.

Since D<sub>iodate</sub> correlates with both stoichiometry and cation ordering, a multivariate regression analysis was performed (Fig. S1), resulting in a P value of < 0.001 and an adjusted  $R^2$  of 0.75. There are several reasons why the multivariate analysis may not accurately describe the relationship between Diodate, stoichiometry, and cation ordering, however. First, there is a collinearity between stoichiometry and cation ordering (the two independent variables) with an R<sup>2</sup> value of 0.87, which suggests that it is not a good practice to use both variables to predict D<sub>iodate</sub>. Second, the regression resulted in a high P value of 0.375 for the relationship between cation ordering and Diodate, suggesting that this relationship in the multivariate analysis is not statistically significant. Third, the analysis yielded a positive coefficient for the cation ordering component of the equation, implying that Diodate increases with cation ordering, which is unrealistic considering the empirical data that show the opposite (Fig. 9C).

Alternatively, a simple linear regression can be used to relate  $D_{iodate}$  to either stoichiometry or cation ordering. Stoichiometry was chosen over cation ordering as a predictor because it results in a lower P value of < 0.001 and a higher  $R^2$  of 0.74:

$$D_{iodate} = -0.1934*MgCO_{3} (mol\%) + 10.0727. \tag{9} \label{eq:polyaleq}$$

The empirical relationship given in Equation 9 was derived using all data plotted in Fig. 9B except the one point that falls off the linear least squares line (denoted by an arrow in Fig. 9B and 9C), which was considered an outlier given that its distance from the line (residual = 1.46) exceeds  $2\sigma$  and because it is influential based on a calculated Cook's distance of 1.10 that exceeds the 4/n cutoff of 0.18 (Cook, 1977). More importantly, both experiments preceding and following the excluded one produced dolomites with lower  $D_{iodate}$  values that are similar to each other (Fig. 9A, 9B, and 9C), which further suggests that the excluded point is an outlier and is probably the result of an unidentified experimental error.

Equation 9 predicts that the D<sub>iodate</sub> of a perfectly stoichiometric dolomite (50 mol% MgCO<sub>3</sub>) is 0.4. To our knowledge, no other study has determined Diodate in dolomite before, thus a comparison with the literature is currently not possible. Instead, we can compare our D<sub>iodate</sub> to that in calcite determined by Lu et al. (2010). Lu et al. (2010) calculated only an equilibrium partition coefficient (I<sub>calcite</sub>/I<sub>solution</sub>), thus we used their data to calculate a nonthermodynamic  $D_{iodate}$  (I/Ca<sub>calcite</sub> / I/Ca<sub>solution</sub>) similar to how we calculated our  $D_{iodate}$ . This yields  $D_{iodate}$  in calcite that ranges between 0.8 and 1.54 (note that all data points are between 0.8 and 1.02 with only one point falling outside this range). Interestingly, the calculated D<sub>iodate</sub> values of Lu et al. (2010) decreases with increasing I/Ca in solution, similar to the trend observed in our Fig. 9A. Importantly, D<sub>iodate</sub> in calcite appears to be at least twice as high as that in dolomite, which implies that dolomite would incorporate half the amount of iodine compared to calcite even if both minerals precipitate from the same solution under identical conditions. While the scenario that a given calcite and dolomite form under identical conditions is both unlikely and difficult to demonstrate, the predication that I/(Ca + Mg) ratios in dolomite should be lower than in calcite is informative and can be used, though with caution, as a general rule of thumb when comparing values across different lithologies.

The finding that Diodate in dolomite is half that in calcite suggests that dolomitization during diagenesis would lead to iodine build up in pore fluids especially given that at least some, if not all, of the iodate released from calcite sediments would be reduced to iodide, which does not get incorporated into dolomite (Fig. 5). Whether iodine in pore fluids continues to increase during diagenesis or whether it eventually precipitates once pore fluids become supersaturated with respect to an iodine-containing mineral is currently unknown. Several iodine-bearing minerals may serve as candidates that could precipitate and sequester iodine from pore fluids including iodyrite (AgI), marshite (CuI), and demicheleite-(I) (BiSI) (e.g., Cooper and Hawthorne, 1997; Demartin et al., 2009; Gołębiowska et al., 2010; Reich et al., 2013). Yet, these minerals are generally rare and, to the best of our knowledge, have not been observed in association with marine carbonates in diagenetic environments. Alternatively, if iodide concentration continues to build up in pore fluids, it may potentially get incorporated into carbonate minerals. However, our study explicitly showed that dolomite does not incorporate iodide (Fig. 5) and Lu et al. (2010) showed the same for calcite, argue against this hypothesis. Importantly, the highest I<sup>-</sup> concentration in our experiments (160 μM; Fig. 5) exceeds those typically observed in pore fluids associated marine sediments in diagenetic environments (typically < 10 μM; Ullman and Aller, 1985; Kennedy and Elderfield, 1987a; Kennedy and Elderfield, 1987b; Anschutz et al.,

2000). We note that much higher values (up to low mM) are observed in pore fluids in deep burial sediments with extreme organic matter accumulation rates, such as the Peru margin (Martin et al., 1993) and methane clathrate localities (Lu et al., 2008). While these settings may host dolomite concretions associated with local alkalinity production from organic carbon remineralization, we posit that these settings are extreme and not representative of the vast majority of sedimentary dolomites in the rock record that formed via replacement of CaCO<sub>3</sub> precursors (Kaczmarek et al., 2017). Given the lower iodine concentrations in carbonate sediments relative to organic matter (Fehn, 2012), carbonate dissolution and minor organic matter oxidation are not expected to increase iodine concentrations in pore fluids significantly. These natural observations, combined with our laboratory observations of no detectable I- partitioning into dolomite (Fig. 5), are strong evidence that detectable dolomite-bound iodine requires  $10^{-3}$  in the fluids from which dolomite precipitated.

# 4.6. Implications for the iodine redox proxy and Precambrian dolomitization

Our experimental results have several implications for using the iodine redox proxy to reconstruct the redox state of the shallow ocean throughout Earth history. First, the observation that dolomite incorporates iodate but not iodide (Fig. 5) suggests that non-zero I/(Ca + Mg) ratios in ancient dolomites are likely the result of the presence of iodate in the dolomitizing fluids whereas a zero I/(Ca + Mg) could indicate dolomite precipitation from anoxic seawater or from reducing pore fluids during diagenesis where the dominant iodine species is iodide. Our observations validate the iodine proxy and are generally consistent with how it has been applied to reconstruct the oceanic redox conditions throughout Earth history (e.g., Lu et al., 2010; Loope et al., 2013; Hardisty et al., 2014; Lu et al., 2016; Hardisty et al., 2017; Lu et al., 2017; Lu et al., 2018; He et al., 2019; Shang et al., 2019; Wie et al., 2019; Worndle et al., 2019; Uahengo et al., 2020). For example, the presence of iodine in dolomites from the Paleoproterozoic can confidently be attributed to iodate accumulation in the shallow ocean, which is related to oxygenation (Hardisty et al., 2014, 2017).

Another implication pertains to the effect of dolomitization in reducing pore fluids on the iodine content in dolomite. Although our experiments were not conducted in reducing fluids, Series A represents experiments whereby iodine-containing sediments were dolomitized in iodine-free fluids (Fig. 4). This experiment approximates diagenetic conditions where sediments that formed under oxic conditions experience dolomitization in iodate-free reducing pore fluids. The observation that the iodine in carbonate sediments was not retained by dolomite (Fig. 4) implies that iodine is not readily rock buffered and that dolomitization in reducing pore fluids could explain the loss of iodine from the carbonate rock record. This means that a zero or low I/(Ca + Mg) in ancient dolomites does not necessarily indicate anoxic conditions in the ocean but could rather reflect dolomitization in reducing pore fluids. Under reducing conditions, iodate is reduced to iodide (Rue et al., 1997; Lu et al., 2016), resulting in dolomite with zero I/(Ca + Mg) since dolomite does not incorporate iodide (Fig. 5). Similar diagenetic trends have been observed in the Great Bahama Bank where I/(Ca + Mg) ratios in the primary aragonite and high-Mg calcite sediments decreased or were completely lost from the diagenetic low-Mg calcite and dolomite (Hardisty et al., 2017). Collectively, our experimental results along with the previous observations from natural settings indicate that I/(Ca + Mg) is unlikely to increase during diagenesis, and thus, corroborate the general assumption that false positives are not expected when using the iodine redox proxy in dolomite.

Given that I/(Ca + Mg) is not easily rock buffered and that our study indicates the potential for complete iodine loss in experiments simulating reducing pore fluids, the presence of iodine at low but non-zero levels in ancient dolomite may provide strong evidence that these dolomites formed under fluid-buffered conditions with at least low iodate. The observation that pore fluid iodate is sourced from seawater and quantitatively reduced during early diagenesis (Kennedy and Elderfield, 1987a; b), supports the interpretation that dolomite formed syndepositionally in exchange with seawater, either directly or via replacement, as proposed by Hardisty et al. (2017). Similar cases for the so-called 'early dolomite' have been previously argued for based on petrographic and geochemical evidence for Precambrian dolomites more broadly (Tucker, 1982; Fairchild et al., 1991; Kah, 2000; van Smeerdijk Hood et al., 2011; cf., Ahm et al., 2019). Collectively, our data support the general premise that Precambrian dolomites are fundamentally different from their Phanerozoic counterparts, which are most commonly replacive (Gregg et al., 2015; Manche and Kaczmarek, 2019, 2021). This warrants caution in using Phanerozoic dolomites as analogs for the Precambrian.

Another related aspect is that while Phanerozoic dolomites show evidence for extensive recrystallization, even during their early diagenetic history and at shallow depths (Gregg et al., 1992; Land, 1992; Al-Aasm and Packard, 2000; Kirmaci, 2008; Al-Aasm et al., 2009; Adams et al., 2019; Veillard et al., 2019; Mueller et al., 2020; Manche and Kaczmarek, 2021; Ryan et al., 2022), the observation that a significant proportion of the Precambrian dolomites exhibit non-zero I/(Ca + Mg) values argue against complete recrystallization. This is not to say that Precambrian dolomites have not undergone recrystallization, but if they have, recrystallization was incapable of completely erasing their depositional signature as evidenced by their iodine content which indiformation under somewhat oxic conditions cates syndepositionally or during early diagenesis.

#### 4.7. Constraints on the redox state of Proterozoic Ocean

The correlation between I/(Ca + Mg) ratios in dolomite and in the solution (Fig. 5) suggests that I/(Ca + Mg)<sub>dolomite</sub> is quantitatively related to [IO<sub>3</sub>] in the solution, which in turn is related to oxygen concentration (Rue et al., 1997; Lu et al., 2016). Our experimental results can therefore be utilized to guide quantitative interpretations of the iodine record. We used the experimentally derived iodate partition coefficient (D<sub>iodate</sub>) and I/(Ca + Mg) values measured in Precambrian dolomites from the literature (Hardisty et al., 2014; Hardisty et al., 2017; Lu et al., 2017; Shang et al., 2019; Wei et al., 2019; He et al., 2020) to reconstruct  $[IO_3]$  in Proterozoic shallow oceans. We focus on the Proterozoic because this Eon witnessed significant environmental perturbations and evolutionary breakthroughs including the Great Oxidation Event, Neoproterozoic Oxidation Event, first appearance of eukaryotes, and diversification of animals (Och and Shields-Zhou, 2012; Lyons et al., 2014; Lyons et al., 2021). Additionally, the Proterozoic iodine record is primarily hosted in dolomite (Hardisty et al., 2014; Hardisty et al., 2017; Lu et al., 2017; Shang et al., 2019; Wei et al., 2019; He et al., 2020).

Given that  $D_{iodate}$  varies with dolomite stoichiometry (Fig. 9C), the bulk Mg/Ca ratios from previous studies (typically reported with I/(Ca + Mg)) were used to calculate stoichiometry, which was then used to adjust  $D_{iodate}$  value via Eq. 9 (Fig. 10). In these calculations, we assumed a modern seawater-like solution with [Mg] of 0.053 M and [Ca] of 0.01 M. Before discussing the data, it must be noted that the reconstructed [ $IO_3$ ] should only be considered as minimum values because the equation used to relate  $D_{iodate}$  to stoichiometry (Eq. 9) is based on values determined via XRD, which is known to overestimate stoichiometry at higher values (Reeder

and Sheppard, 1984), whereas the stoichiometries used to calculate [IO<sub>3</sub>] are derived from the Mg/Ca ratios measured via ICPMS. The data presented in Fig. 10 demonstrate that dolomite stoichiometry plays a significant role in the calculations of [IO<sub>3</sub>] because stoichiometry dictates the value of the partition coefficient (Fig. 9C and 9D). As such, the highest I/(Ca + Mg) values in dolomite may not necessarily translate to high [IO3] when stoichiometry is low. Similarly, relatively low I/(Ca + Mg) values could result in high [IO<sub>3</sub>] when stoichiometry is high (Fig. 10). Accordingly, absolute I/(Ca + Mg) ratios can be misleading if the stoichiometry of the hosting dolomite is not considered. Compounding the need to consider our [IO<sub>3</sub>] estimates as minimum values, our experiments also indicate that diagenetic recrystallization will result in decreased I/(Ca + Mg), which would additionally decrease estimates of [IO<sub>3</sub>]. Therefore, one caveat to the following discussion is that intervals with zero or low I/(Ca + Mg) values may not indicate low oxygen levels but loss of iodine from dolomite during diagenesis. In this context, future studies may benefit from utilizing Ca and Mg isotopes to distinguish fluid- vs sediment-buffered dolomites (e.g., Ahm et al., 2019), which, along with our experimental constraints showing that iodine is not easily rock-buffered, may lead to more accurate reconstructions of oxygen levels in the ocean.

In interpreting the calculated [IO<sub>3</sub>] values (Fig. 11), IO<sub>3</sub> and oxygen depth profiles from modern seawater (Lu et al., 2016) will be considered as analogues. These profiles show that an IO<sub>3</sub> value of < 0.25 μM corresponds to oxygen-depleted water with concentration of < 20 - 70 µmol/kg (Lu et al., 2016). Above this cutoff, [IO<sub>3</sub>] is largely dictated by primary production and local mixing patterns (Lu et al., 2016; Chance et al., 2014; Hardisty et al., 2021). Turning now to the iodine record, the Archean is characterized by zero I/(Ca + Mg) ratios (Fig. 11) that have been suggested to reflect anoxic conditions in the shallow ocean (Hardisty et al., 2014). Our observation that only  $IO_3^-$  is incorporated into dolomite supports this interpretation and further suggests that the reduced species of iodine, iodide, was the dominant form in seawater. The first peak in I/(Ca + Mg) occurs at  $\sim 2.45 - 2.40$  Ga at the onset of the Great Oxidation Event (GOE) (Fig. 11). Our calculations show that this peak corresponds to very low levels of IO<sub>3</sub> in the shallow ocean ( $\sim$ 0.07  $\mu$ M), which either indicate anoxia or levels of oxygen insufficient to stabilize and support the accumulation of modernlike marine IO3. Based on the understanding of the GOE as a transitory episode characterized by oscillating atmospheric oxygen levels until the onset of the Lomagundi carbon isotope excursion (Lyons et al., 2014; Poulton et al., 2021) rather than an abrupt event, our calculations suggest an anoxic or very poorly oxygenated shallow ocean at the early stages of the GOE. Recent constraints based on mass independent fractionation of sulfur isotopes suggest that the irreversible and permanent increase in atmospheric oxygenation did not occur until  $\sim$  2.22 Ga (Poulton et al., 2021). Accordingly, a poorly oxygenated shallow ocean before 2.22 Ga, as suggested by our calculations, is likely, though the observed increase in I/(Ca + Mg) at  $\sim 2.45 - 2.40$  may be the result of a transient and local oxygen accumulation in the shallow ocean that was in disequilibrium with the then low oxygen atmosphere (Hardisty et al., 2014).

An increase in atmospheric oxygen is interpreted to have occurred during the Lomagundi Event (Bekker and Holland, 2012; Poulton et al., 2021), but we note that, beyond one data point, there is no clear evidence for relatively higher IO<sub>3</sub> above that found in modern oxygen minimum zones during this interval. Indeed, though there are notable oscillations in IO<sub>3</sub> during the Paleo- and meso-Proterozoic, [IO<sub>3</sub>] values stay clearly near or below this modern OMZ range. Our calculations support the hypothesis that during the majority of the Proterozoic broadly between 1.8 and 0.8 Ga (i.e., the Boring Billion) the shallow ocean

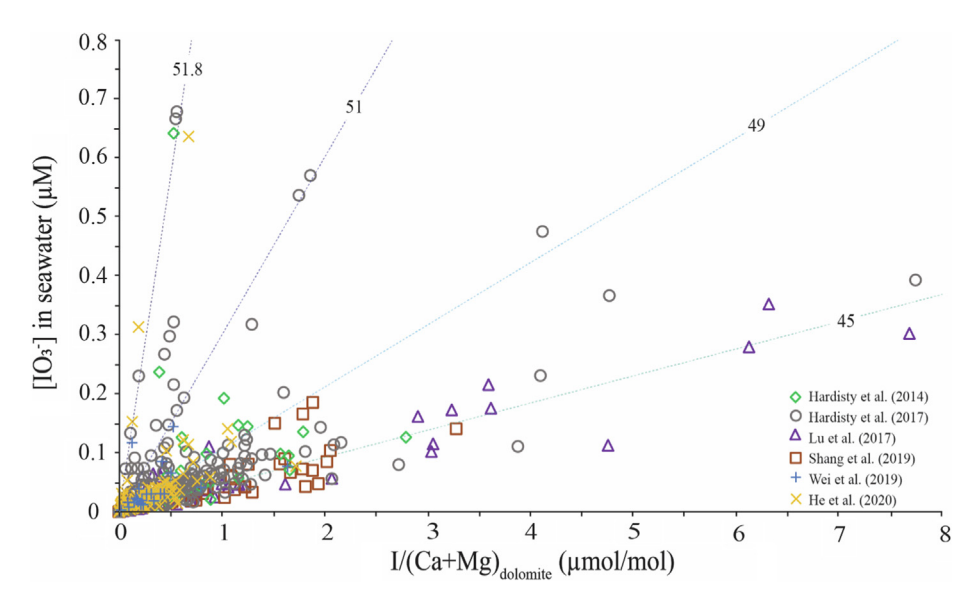


Fig. 10. I/(Ca + Mg) values from Proterozoic dolomites plotted against the calculated seawater  $[IO_3^*]$  using the experimentally derived partition coefficient of iodate ( $D_{iodate}$ ). The dashed lines and numbers refer to dolomite stoichiometry, which was used to adjust  $D_{iodate}$  according to Eq. 9.

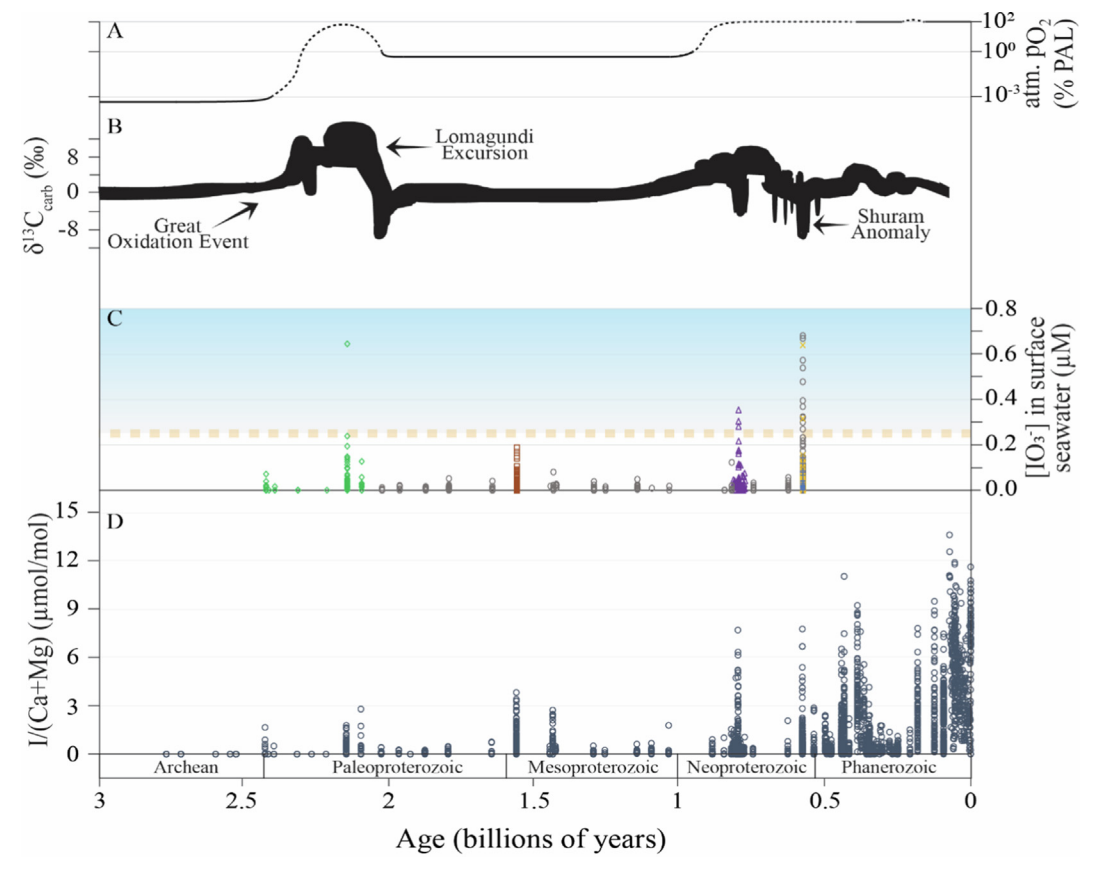


Fig. 11. Compilations of proxy records through time. (A) the secular variation in atmospheric oxygen in % relative to Present Atmospheric Level (PAL) modified after Lyons et al. (2014). (B) the carbonate  $\delta^{13}$ C record through time modified after Planavsky et al. (2012). (C) [IO<sub>3</sub>] in Proterozoic shallow ocean calculated in this study. The legend for data in panel (C) is provided in Fig. 10. (D) I/(Ca + Mg) ratios from dolostones and limestones compiled from the literature (Lu et al., 2010; Loope et al., 2013; Hardisty et al., 2014; Zhou et al., 2015; Hardisty et al., 2017; Lu et al., 2017; Lu et al., 2017; Edwards et al., 2018; Shang et al., 2019; Wei et al., 2019; Wörndle et al., 2019; Young et al., 2019; Bowman et al., 2020; He et al., 2020; Bowman et al., 2021; Pohl et al., 2021). All Proterozoic I/(Ca + Mg) data were used to calculate [IO<sub>3</sub>] except data without separate Mg/Ca ratios. We also excluded samples whose Mg/Ca ratio < 0.6 mol/mol, which corresponds to a stoichiometry of < 37.5 mol% MgCO<sub>3</sub>. This arbitrary cutoff was used so that only dolomite samples are considered and because our experiments produced dolomites with > ~ 45 mol % stoichiometry and are thus not applicable to phases with much lower stoichiometries. The horizontal dashed line in panel C represents [IO<sub>3</sub>] = 0.25 μM. Based on modern analogs, values below this cutoff indicate oxygen-depleted water with O<sub>2</sub> concentration < 20–70 μmol/kg (Lu et al., 2016).

was generally poorly oxygenated. This is consistent with Ce/Ce\* anomaly records that suggest low oxygen levels in the shallow ocean during the Mesoproterozoic (Tang et al., 2016; Liu et al., 2021), as well as atmospheric O<sub>2</sub> estimates based on Cr isotopes, which point to  $pO_2$  levels of < 1 % PAL (Present Atmospheric Level) until ~ 0.8 Ga (Crowe et al., 2013; Planavsky et al., 2014; Planavsky et al., 2018; Colwyn et al., 2019). In comparison to the suggested low oxygen levels during the Boring Billion, our calculations suggest that the I/(Ca + Mg) peaks in the Neoproterozoic during Bitter Springs Anomaly (Lu et al., 2017) and Shuram Anomaly (Hardisty et al., 2017) correspond to  $[IO_3^-] > 0.25 \mu M$ , suggesting a well oxygenated shallow ocean after the Neoproterozoic Oxygenation Event (NOE) (Och and Shields-Zhou, 2012). However, both calcite and dolomite I/(Ca + Mg) records support that this was not a permanent transition (e.g., Lu et al., 2018). Finally, our calculations lend support to the proposition that challenging environmental conditions in the shallow ocean during the majority of the Proterozoic may have delayed the evolution of O2-dependent life (Planavsky et al., 2014; Reinhard et al., 2016; Lyons et al., 2021).

#### 5. Conclusions

High-temperature laboratory dolomitization experiments demonstrate that iodate - the oxidized species of iodine - is incorporated into dolomite, whereas iodide - the reduced species - is not. These observations represent the first validation for the iodine proxy in dolomite and suggest that non-zero I/(Ca + Mg) in ancient dolomites reflect the presence of iodate, and thus oxygen, in the dolomitizing fluid. The experimental results further show that reaction temperature does not appear to impact iodine incorporation over the investigated temperature range of 170-200 °C. This observation supports the applicability of high-temperature experiments to natural dolomites that form at lower temperature. We acknowledge, however, that the investigated range of temperature is quite narrow and should be expanded in future work. Furthermore, the experiments show that the I/(Ca + Mg) of dolomite is related quantitatively to the concentration of iodate in the solution, permitting the calculation of a partition coefficient for iodate (D<sub>iodate</sub>) in dolomite which relates I/(Ca + Mg) in dolomite and in solution. The results show that iodine incorporation into dolomite is dependent on the major cation composition and structure arrangement of cations in the dolomite. Specifically, that I/(Ca + Mg) in dolomite decreases with increasing dolomite stoichiometry and cation ordering.

The experimentally derived  $D_{iodate}$  was used in conjunction with I/(Ca+Mg) measurements from Proterozoic dolomites reported in the literature to calculate  $[IO_3^*]$  in the shallow ocean. Our calculations support the initial accumulation of shallow ocean iodate during the later stages of the Great Oxidation Event after the onset of the Lomagundi Excursion. Subsequently, our data show that the vast majority of the Proterozoic (i.e., the Boring Billion) was characterized by persistently low levels of iodate, and likely, as the proxy suggests, low levels of oxygen, until  $\sim 0.8$  Ga, when iodate levels increased to modern-like values from well-oxygenated settings.

#### **Data availability**

Data is available as a supplemental file

# **Declaration of Competing Interest**

The authors declare that they have no known competing financial interests or personal relationships that could have appeared to influence the work reported in this paper.

#### Acknowledgements

This study was funded by a student research grant (Gerald M. Friedman Endowment) awarded by the SEPM Foundation to MSH and a student research grant awarded by the Graduate College of Western Michigan University to MSH. During the writing of this article, MSH was supported by Schlanger Fellowship awarded to him by the U.S. Science Support Program (USSSP) and by the Post-doctoral Scholar Program at Woods Hole Oceanographic Institution. JEB is supported by NSF Ocean Sciences Postdoctoral Fellowship (Award # 2126568). DSH acknowledges support from NSF CO award # 1829406. SEK acknowledges partial support by a grant from NSF (EAR-SGP-1828880). We would like to thank three anonymous reviewers and Associate Editor Dr. Nicholas Tosca for their helpful feedback, which improved our manuscript appreciably.

#### Appendix A. Supplementary material

Supplementary material to this article can be found online at https://doi.org/10.1016/j.gca.2022.10.027.

#### References

Adams, A., Diamond, L.W., Aschwanden, L., 2019. Dolomitization by hypersaline reflux into dense groundwaters as revealed by vertical trends in strontium and oxygen isotopes: Upper Muschelkalk, Switzerland. Sedimentology 66 (1), 362–300

Ahm, A.S.C., Maloof, A.C., Macdonald, F.A., Hoffman, P.F., Bjerrum, C.J., Bold, U., Rose, C.V., Strauss, J.V., Higgins, J.A., 2019. An early diagenetic deglacial origin for basal Ediacaran "cap dolostones". Earth Planet. Sci. Lett. 506, 292–307.

Al-Aasm, I.S., Packard, J.J., 2000. Stabilization of early-formed dolomite: a tale of divergence from two Mississippian dolomites. Sed. Geol. 131 (3–4), 97–108.

Al-Aasm, I.S., Ghazban, F., Ranjbaran, M., 2009. Dolomitization and related fluid evolution in the Oligocene-Miocene Asmari Formation, Gachsaran area, SW Iran: petrographic and isotopic evidence. J. Pet. Geol 32 (3), 287–304.

Alkhatib, M., Qutob, M., Alkhatib, S., Eisenhauer, A., 2022. Influence of precipitation rate and temperature on the partitioning of magnesium and strontium in calcite overgrowths. Chem. Geol. 120841

Anschutz, P., Sundby, B., Lefrancois, L.U.C.I.E., Luther III, G.W., Mucci, A., 2000. Interactions between metal oxides and species of nitrogen and iodine in bioturbated marine sediments. Geochim. Cosmochim. Acta 64 (16), 2751–2763.

Arvidson, R.S., Mackenzie, F.T., 1999. The dolomite problem; control of precipitation kinetics by temperature and saturation state. Am. J. Sci. 299 (4), 257–288.

Avrami, M., 1939. Kinetics of phase change. I General theory. J. Chem. Phys. 7 (12), 1103–1112.

Beattie, P., Drake, M., Jones, J., Leeman, W., Longhi, J., McKay, G., Nielsen, R., Palme, H., Shaw, D., Takahashi, E., Watson, B., 1993. Terminology for trace-element partitioning. Geochim. Cosmochim. Acta 57 (7), 1605–1606.

Bekker, A., Holland, H.D., 2012. Oxygen overshoot and recovery during the early Paleoproterozoic. Earth Planet. Sci. Lett. 317, 295–304.

Berthelot, M., 1872. On the law which governs the distribution of a substance between two solvents. Ann Chim Phys 4th series), 26, 408–417.

Bowman, C.N., Lindskog, A., Kozik, N.P., Richbourg, C.G., Owens, J.D., Young, S.A., 2020. Integrated sedimentary, biotic, and paleoredox dynamics from multiple localities in southern Laurentia during the late Silurian (Ludfordian) extinction event. Palaeogeogr. Palaeoclimatol. Palaeoecol. 553, 109799.

Bowman, C.N., Them II, T.R., Knight, M.D., Kaljo, D., Eriksson, M.E., Hints, O., Martma, T., Owens, J.D., Young, S.A., 2021. A multi-proxy approach to constrain reducing conditions in the Baltic Basin during the late Silurian Lau carbon isotope excursion. Palaeogeogr. Palaeoclimatol. Palaeoecol. 581, 110624.

Broecker, W.S., Peng, T.-H., 1982. Tracers in the sea. Lamont-Doherty Geological Observatory, New York, p. 690 p.

Budd, D.A., 1997. Cenozoic dolomites of carbonate islands: their attributes and origin. Earth Sci. Rev. 42 (1–2), 1–47.

Cantine, M.D., Knoll, A.H., Bergmann, K.D., 2020. Carbonates before skeletons: A database approach. Earth Sci. Rev. 201 103065.

Colwyn, D.A., Sheldon, N.D., Maynard, J.B., Gaines, R., Hofmann, A., Wang, X., Gueguen, B., Asael, D., Reinhard, C.T., Planavsky, N.J., 2019. A paleosol record of the evolution of Cr redox cycling and evidence for an increase in atmospheric oxygen during the Neoproterozoic. Geobiology 17 (6), 579–593.

Cook, R.D., 1977. Detection of influential observation in linear regression. Technometrics 19 (1), 15–18.

Cooper, M.A., Hawthorne, F.C., 1997. A note on the crystal structure of marshite. The Canadian Mineralogist 35 (3), 785–786.

Crowe, S.A., Døssing, L.N., Beukes, N.J., Bau, M., Kruger, S.J., Frei, R., Canfield, D.E., 2013. Atmospheric oxygenation three billion years ago. Nature 501 (7468), 535–538.

- Cutter, G.A., Moffett, J.W., Nielsdóttir, M.C., Sanial, V., 2018. Multiple oxidation state trace elements in suboxic waters off Peru: In situ redox processes and advective/diffusive horizontal transport. Mar. Chem. 201, 77-89.
- Demartin, F., Gramaccioli, C.M., Campostrini, I., 2009. Demicheleite-(Cl), BiSCl, a new mineral from La Fossa crater, Vulcano, Aeolian Islands. Italy. American Mineralogist 94 (7), 1045-1048.
- Edwards, C.T., Fike, D.A., Saltzman, M.R., Lu, W., Lu, Z., 2018. Evidence for local and global redox conditions at an Early Ordovician (Tremadocian) mass extinction. Earth Planet. Sci. Lett. 481, 125-135.
- Emerson, S., Cranston, R.E., Liss, P.S., 1979. Redox species in a reducing fjord: equilibrium and kinetic considerations. Deep Sea Res. Part A 26 (8), 859-878.
- Fairchild, I.J., Knoll, A.H., Swett, K., 1991. Coastal lithofacies and biofacies associated with syndepositional dolomitization and silicification (Draken Formation, Upper Riphean, Svalbard). Precambr. Res. 53 (3-4), 165-197.
- Fehn, U., 2012. Tracing crustal fluids: Applications of natural 129I and 36Cl. Annu. Rev. Earth Planet. Sci. 40, 45-67.
- Gabitov, R.I., Sadekov, A., Leinweber, A., 2014. Crystal growth rate effect on Mg/Ca and Sr/Ca partitioning between calcite and fluid: An in situ approach. Chem. Geol. 367, 70-82.
- Given, R.K., Wilkinson, B.H., 1987. Dolomite abundance and stratigraphic age; constraints on rates and mechanisms of Phanerozoic dolostone formation. J. Sediment. Res. 57 (6), 1068-1078.
- Goldsmith, J.R., Graf, D.L., 1958. Structural and compositional variations in some natural dolomites. J. Geol. 66 (6), 678-693.
- Gołębiowska, B., Pieczka, A., Rzepa, G., Matyszkiewicz, J., Krajewski, M., 2010. lodargyrite from Zalas (Cracow area, Poland) as an indicator of Oligocene-Miocene aridity in Central Europe. Palaeogeogr. Palaeoclimatol. Palaeoecol. 296 (1-2), 130-137.
- Gran, G., 1952. Determination of the equivalence point in potentiometric titrations. Part II. Analyst 77 (920), 661-671.
- Gregg, J.M., Howard, S.A., Mazzullo, S.J., 1992. Early diagenetic recrystallization of Holocene (< 3000 years old) peritidal dolomites, Ambergris Cay. Belize. Sedimentology 39 (1), 143-160.
- Gregg, J.M., Bish, D.L., Kaczmarek, S.E., Machel, H.G., 2015. Mineralogy, nucleation and growth of dolomite in the laboratory and sedimentary environment: a review. Sedimentology 62 (6), 1749-1769.
- Hardisty, D.S., Lu, Z., Planavsky, N.J., Bekker, A., Philippot, P., Zhou, X., Lyons, T.W., 2014. An iodine record of Paleoproterozoic surface ocean oxygenation. Geology 42 (7), 619-622.
- Hardisty, D.S., Lu, Z., Bekker, A., Diamond, C.W., Gill, B.C., Jiang, G., Kah, L.C., Knoll, A. H., Loyd, S.J., Osburn, M.R., Planavsky, N.J., 2017. Perspectives on Proterozoic surface ocean redox from iodine contents in ancient and recent carbonate. Earth Planet. Sci. Lett. 463, 159-170.
- Hardisty, D.S., Horner, T.J., Evans, N., Moriyasu, R., Babbin, A.R., Wankel, S.D., Moffett, J.W., Nielsen, S.G., 2021. Limited iodate reduction in shipboard seawater incubations from the Eastern Tropical North Pacific oxygen deficient zone. Earth Planet. Sci. Lett. 554, 116676.
- Hashim, M.S., Kaczmarek, S.E., 2020. Experimental stabilization of carbonate sediments to calcite: Insights into the depositional and diagenetic controls on calcite microcrystal texture. Earth Planet. Sci. Lett. 538, 116235.
- Hashim, M.S., Kaczmarek, S.E., 2021a. Evolution of calcite microcrystal morphology during experimental dissolution. J. Sediment. Res. 91 (3), 229-242.
- Hashim, M.S., Kaczmarek, S.E., 2021b. The transformation of aragonite to calcite in the presence of magnesium: Implications for marine diagenesis. Earth Planet. Sci. Lett. 574, 117166.
- He, R., Jiang, G., Lu, W., Lu, Z., 2020. Iodine records from the Ediacaran Doushantuo cap carbonates of the Yangtze Block. South China. Precambrian Research 347,
- Henderson, L.M., Kracek, F.C., 1927. The fractional precipitation of barium and radium chromates. J. Am. Chern. Soc. 49, 739-749.
- Hood, A.V., Wallace, M.W., Drysdale, R.N., 2011. Neoproterozoic aragonite-dolomite seas? Widespread marine dolomite precipitation in Cryogenian reef complexes. Geology 39 (9), 871-874.
- Ishikawa, M., Ichikuni, M., 1984. Uptake of sodium and potassium by calcite. Chem. Geol. 42 (1-4), 137-146.
- Jacobson, R.L., Usdowski, H.E., 1976. Partitioning of strontium between calcite, dolomite and liquids: An experimental study under higher temperature diagenetic conditions, and a model for the prediction of mineral pairs for geothermometry. Contrib. Miner. Petrol. 59 (2), 171–185.
- Johnson, J.W., Oelkers, E.H., Helgeson, H.C., 1992. SUPCRT92: A software package for calculating the standard molal thermodynamic properties of minerals, gases, aqueous species, and reactions from 1 to 5000 bar and 0 to 1000 C. Comput. Geosci, 18 (7), 899–947.
- Kaczmarek, S.E., Gregg, J.M., Bish, D.L., Machel, H.G., Fouke, B.W., 2017. Dolomite, very-high magnesium calcite, and microbes: implications for the microbial model of dolomitization. In: Characterization and Modeling of Carbonates-Mountjoy Symposium, vol. 1, pp. 7-20.
- Kaczmarek, S.E., Sibley, D.F., 2007. A comparison of nanometer-scale growth and dissolution features on natural and synthetic dolomite crystals: implications for the origin of dolomite. J. Sediment. Res. 77 (5), 424–432.
- Kaczmarek, S.E., Sibley, D.F., 2011. On the evolution of dolomite stoichiometry and cation order during high-temperature synthesis experiments: an alternative model for the geochemical evolution of natural dolomites. Sed. Geol. 240 (1-2), 30-40
- Kaczmarek, S.E., Sibley, D.F., 2014. Direct physical evidence of dolomite recrystallization. Sedimentology 61 (6), 1862-1882.

- Kaczmarek, S.E., Thornton, B.P., 2017. The effect of temperature on stoichiometry, cation ordering, and reaction rate in high-temperature dolomitization experiments. Chem. Geol. 468, 32-41.
- Kah, L.C., 2000. Depositional δ180 signatures in Proterozoic dolostones: constraints on seawater chemistry and early diagenesis.
- Katz, A., Matthews, A., 1977. The dolomitization of CaCO3: an experimental study at 252-295° C. Geochim. Cosmochim. Acta 41 (2), 297-308.
- Kell-Duivestein, I.J., Baldermann, A., Mavromatis, V., Dietzel, M., 2019. Controls of temperature, alkalinity and calcium carbonate reactant on the evolution of dolomite and magnesite stoichiometry and dolomite cation ordering degree-An experimental approach. Chem. Geol. 529, 119292.
- Kennedy, H.A., Elderfield, H., 1987a. Iodine diagenesis in pelagic deep-sea sediments. Geochim. Cosmochim. Acta 51 (9), 2489-2504.
- Kennedy, H.A., Elderfield, H., 1987b. Iodine diagenesis in non-pelagic deep-sea sediments. Geochim. Cosmochim. Acta 51 (9), 2505-2514.
- Kerisit, S.N., Smith, F.N., Saslow, S.A., Hoover, M.E., Lawter, A.R., Qafoku, N.P., 2018. Incorporation modes of iodate in calcite. Environ. Sci. Technol. 52 (10), 5902-
- Kirmaci, M.Z., 2008. Dolomitization of the late cretaceous-paleocene platform carbonates, gölköy (Ordu), eastern pontides. NE Turkey. Sedimentary Geology 203 (3-4), 289-306.
- Land, L.S., 1985. The origin of massive dolomite. J. Geol. Educ. 33 (2), 112-125.
- Land, L.S., 1992. The dolomite problem: stable and radiogenic isotope clues. In: Isotopic Signatures and Sedimentary Records. Springer, Berlin, Heidelberg, pp.
- Land, L.S., 1998. Failure to Precipitate Dolomite at 25 C fromDilute Solution Despite 1000-Fold Oversaturation after 32 Years. Aquat. Geochem. 4 (3), 361-
- Li, F., Webb, G.E., Algeo, T.J., Kershaw, S., Lu, C., Oehlert, A.M., Gong, Q., Pourmand, A., Tan, X., 2019. Modern carbonate ooids preserve ambient aqueous REE signatures. Chem. Geol. 509, 163-177.
- Loope, G.R., Kump, L.R., Arthur, M.A., 2013. Shallow water redox conditions from the Permian-Triassic boundary microbialite: The rare earth element and iodine geochemistry of carbonates from Turkey and South China. Chem. Geol. 351,
- Lu, Z., Jenkyns, H.C., Rickaby, R.E., 2010. Iodine to calcium ratios in marine carbonate as a paleo-redox proxy during oceanic anoxic events. Geology 38 (12), 1107-
- Lu, Z., Hoogakker, B.A., Hillenbrand, C.D., Zhou, X., Thomas, E., Gutchess, K.M., Lu, W., Jones, L., Rickaby, R.E., 2016. Oxygen depletion recorded in upper waters of the glacial Southern Ocean. Nat. Commun. 7 (1), 1–9.
- Lu, Z., Lu, W., Rickaby, R.E., Thomas, E., 2020. Earth History of Oxygen and the iprOxy. Cambridge University Press.
- Lu, W., Wörndle, S., Halverson, G.P., Zhou, X., Bekker, A., Rainbird, R.H., Hardisty, D. S., Lyons, T.W., Lu, Z., 2017. Iodine proxy evidence for increased ocean oxygenation during the Bitter Springs Anomaly. Geochem. Perspect. Lett. 5, 53-57.
- Lu, W., Ridgwell, A., Thomas, E., Hardisty, D.S., Luo, G., Algeo, T.J., Saltzman, M.R., Gill, B.C., Shen, Y., Ling, H.F., Edwards, C.T., 2018. Late inception of a resiliently oxygenated upper ocean. Science 361 (6398), 174-177.
- Lu, Z., Tomaru, H., Fehn, U., 2008. Iodine ages of pore waters at Hydrate Ridge (ODP Leg 204), Cascadia Margin: Implications for sources of methane in gas hydrates. Earth Planet. Sci. Lett. 267 (3–4), 654–665.
- Lumsden, D.N. and Chimahusky, J.S., 1980. Relationship between dolomite
- nonstoichiometry and carbonate facies parameters. Lyons, T.W., Reinhard, C.T., Planavsky, N.J., 2014. The rise of oxygen in Earth's early ocean and atmosphere. Nature 506 (7488), 307–315.
- Lyons, T.W., Diamond, C.W., Planavsky, N.J., Reinhard, C.T., Li, C., 2021. Oxygenation, life, and the planetary system during Earth's middle history: An overview. Astrobiology 21 (8), 906-923.
- Machel, H.G., 2004. Concepts and models of dolomitization: a critical reappraisal. Geological Society, London, Special Publications 235 (1), 7–63.
- Malone, M.J., Baker, P.A., Burns, S.J., 1996. Recrystallization of dolomite: An experimental study from. Geochim. Cosmochim. Acta 60 (12), 2189–2207. Manche, C.J., Kaczmarek, S.E., 2019. Evaluating reflux dolomitization using a novel
- high-resolution record of dolomite stoichiometry: a case study from the Cretaceous of central Texas, USA. Geology 47 (6), 586-590.
- Manche, C.J., Kaczmarek, S.E., 2021. A global study of dolomite stoichiometry and cation ordering through the Phanerozoic. J. Sediment. Res. 91 (5), 520-546.
- Martin, J.B., Gieskes, J.M., Torres, M., Kastner, M., 1993. Bromine and iodine in Peru margin sediments and pore fluids: Implications for fluid origins. Geochim. Cosmochim. Acta 57 (18), 4377-4389.
- Mavromatis, V., Gautier, Q., Bosc, O., Schott, J., 2013. Kinetics of Mg partition and Mg stable isotope fractionation during its incorporation in calcite. Geochim. Cosmochim. Acta 114, 188-203.
- McIntire, W.L., 1963. Trace element partition coefficients—a review of theory and applications to geology. Geochim. Cosmochim. Acta 27 (12), 1209-1264.
- Montanez, I.P., Read, J.F., 1992. Fluid-rock interaction history during stabilization of early dolomites, Upper Knox Group (Lower Ordovician), US Appalachians. J. Sediment. Res. 62 (5), 753-778.
- Moriyasu, R., Evans, N., Bolster, K.M., Hardisty, D.S., Moffett, J.W., 2020. The distribution and redox speciation of iodine in the Eastern Tropical North Pacific Ocean. Global Biogeochem. Cycles 34 (2).
- Morse, J.W., 1974. Dissolution kinetics of calcium carbonate in sea water; III, A new method for the study of carbonate reaction kinetics. Am. J. Sci. 274 (2), 97-107.

- Morse, J.W., Andersson, A.J., Mackenzie, F.T., 2006. Initial responses of carbonaterich shelf sediments to rising atmospheric pCO2 and "ocean acidification": Role of high Mg-calcites. Geochim. Cosmochim. Acta 70 (23), 5814–5830.
- Morse, J.W., Bender, M.L., 1990. Partition coefficients in calcite: Examination of factors influencing the validity of experimental results and their application to natural systems. Chem. Geol. 82, 265–277.
- Morse, J.W., Mackenzie, F.T., 1990. Geochemistry of sedimentary carbonates. Elsevier.
- Mucci, A., 1987. Influence of temperature on the composition of magnesian calcite overgrowths precipitated from seawater. Geochim. Cosmochim. Acta 51 (7), 1977–1984.
- Mucci, A., Morse, J.W., 1983. The incorporation of Mg2+ and Sr2+ into calcite overgrowths: influences of growth rate and solution composition. Geochim. Cosmochim. Acta 47 (2), 217–233.
- Mueller, M., Igbokwe, O.A., Walter, B., Pederson, C.L., Riechelmann, S., Richter, D.K., Albert, R., Gerdes, A., Buhl, D., Neuser, R.D., Bertotti, G., 2020. Testing the preservation potential of early diagenetic dolomites as geochemical archives. Sedimentology 67 (2), 849–881.
- Nernst, W., 1891. Distribution of a substance between two solvents and between solvent and vapor. Z. Phys. Them. 8, 110–139.
- Nordeng, S.H., Sibley, D.F., 1994. Dolomite stoichiometry and Ostwald's step rule. Geochim. Cosmochim. Acta 58 (1), 191–196.
- Och, L.M., Shields-Zhou, G.A., 2012. The Neoproterozoic oxygenation event: Environmental perturbations and biogeochemical cycling. Earth Sci. Rev. 110 (1–4), 26–57.
- Ohde, S., Kitano, Y., 1984. Coprecipitation of strontium with marine Ca-Mg carbonates. Geochem. J. 18 (3), 143–146.
- Owens, J.D., Lyons, T.W., Hardisty, D.S., Lowery, C.M., Lu, Z., Lee, B., Jenkyns, H.C., 2017. Patterns of local and global redox variability during the Cenomanian–Turonian Boundary Event (Oceanic Anoxic Event 2) recorded in carbonates and shales from central Italy. Sedimentology 64 (1), 168–185.
- Parkhurst, D.L., Appelo, C.A.J., 2013. Description of input and examples for PHREEQC version 3—a computer program for speciation, batch-reaction, one-dimensional transport, and inverse geochemical calculations. US geological survey techniques and methods 6 (A43), 497.
- Pitzer, K.S., Press, C.R.C. (Eds.), 1991. Activity Coefficients in Electrolyte Solutions (Vol. 2). CRC Press, Boca Raton, FL.
- Planavsky, N.J., Bekker, A., Hofmann, A., Owens, J.D., Lyons, T.W., 2012. Sulfur record of rising and falling marine oxygen and sulfate levels during the Lomagundi event. Proc. Natl. Acad. Sci. 109 (45), 18300–18305.
- Planavsky, N.J., Reinhard, C.T., Wang, X., Thomson, D., McGoldrick, P., Rainbird, R.H., Johnson, T., Fischer, W.W., Lyons, T.W., 2014. Low Mid-Proterozoic atmospheric oxygen levels and the delayed rise of animals. Science 346 (6209), 635–638.
- Planavsky, N.J., Cole, D.B., Isson, T.T., Reinhard, C.T., Crockford, P.W., Sheldon, N.D., Lyons, T.W., 2018. A case for low atmospheric oxygen levels during Earth's middle history. Emerging Topics in Life Sciences 2 (2), 149–159.
- Pohl, A., Lu, Z., Lu, W., Stockey, R.G., Elrick, M., Li, M., Desrochers, A., Shen, Y., He, R., Finnegan, S., Ridgwell, A., 2021. Vertical decoupling in Late Ordovician anoxia due to reorganization of ocean circulation. Nat. Geosci. 14 (11), 868–873.
- Reeder, R.J., Sheppard, C.E., 1984. Variation of lattice parameters in some sedimentary dolomites. Am. Mineral. 69 (5–6), 520–527.
- Reeder, R.J., Wenk, H.R., 1983. Structure refinements of some thermally disordered dolomites. Am. Mineral. 68 (7–8), 769–776.
- Reich, M., Snyder, G.T., Álvarez, F., Pérez, A., Palacios, C., Vargas, G., Cameron, E.M., Muramatsu, Y., Fehn, U., 2013. Using iodine isotopes to constrain supergene fluid sources in arid regions: insights from the Chuquicamata oxide blanket. Econ. Geol. 108 (1), 163–171.
- Reinhard, C.T., Planavsky, N.J., Olson, S.L., Lyons, T.W., Erwin, D.H., 2016. Earth's oxygen cycle and the evolution of animal life. Proc. Natl. Acad. Sci. 113 (32), 8933–8938.
- Rue, E.L., Smith, G.J., Cutter, G.A., Bruland, K.W., 1997. The response of trace element redox couples to suboxic conditions in the water column. Deep Sea Res. Part I 44 (1), 113–134.
- Ryan, B.H., Kaczmarek, S.E., Rivers, J.M., Manche, C.J., 2022. Extensive recrystallization of Cenozoic dolomite during shallow burial: A case study from the Palaeocene-Eocene Umm er Radhuma Formation and a global metaanalysis. Sedimentology.

- Seyedali, M., Coogan, L.A., Gillis, K.M., 2021. The effect of solution chemistry on elemental and isotopic fractionation of lithium during inorganic precipitation of calcite. Geochim. Cosmochim. Acta 311, 102–118.
- Shang, M., Tang, D., Shi, X., Zhou, L., Zhou, X., Song, H., Jiang, G., 2019. A pulse of oxygen increase in the early Mesoproterozoic ocean at ca. 1.57–1.56 Ga. Earth Planet. Sci. Lett. 527, 115797.
- Sibley, D.F., Dedoes, R.E., Bartlett, T.R., 1987. Kinetics of dolomitization. Geology 15 (12), 1112–1114.
- Sibley, D.F., Nordeng, S.H., Borkowski, M.L., 1994. Dolomitization kinetics of hydrothermal bombs and natural settings. J. Sediment. Res. 64 (3a), 630–637.
- Smrzka, D., Zwicker, J., Bach, W., Feng, D., Himmler, T., Chen, D., Peckmann, J., 2019. The behavior of trace elements in seawater, sedimentary pore water, and their incorporation into carbonate minerals: A review. Facies 65 (4), 1–47.
- Swart, P.K., 2015. The geochemistry of carbonate diagenesis: The past, present and future. Sedimentology 62 (5), 1233–1304.
- Tang, J., Köhler, S.J., Dietzel, M., 2008. Sr2+/Ca2+ and 44Ca/40Ca fractionation during inorganic calcite formation: I, Sr incorporation. Geochim. Cosmochim. Acta 72 (15), 3718–3732.
- Teoh, C.P., Laya, J.C., Rose, K., Kaczmarek, S., 2022. The effects of magnesium concentration in high-magnesium calcite allochems on dolomitization: Insights from high-temperature dolomite synthesis experiments. J. Sediment. Res. 92 (2), 134–143.
- Tucker, M.E., 1982. Precambrian dolomites: petrographic and isotopic evidence that they differ from Phanerozoic dolomites. Geology 10 (1), 7–12.
- Uahengo, C.I., Shi, X., Jiang, G., Vatuva, A., 2020. Transient shallow-ocean oxidation associated with the late Ediacaran Nama skeletal fauna: evidence from iodine contents of the Lower Nama Group, southern Namibia. Precambr. Res. 343, 105732
- Ullman, W.J., Aller, R.C., 1985. The geochemistry of iodine in near-shore carbonate sediments. Geochim. Cosmochim. Acta 49 (4), 967–978.
- Vahrenkamp, V.C., Swart, P.K., 1990. New distribution coefficient for the incorporation of strontium into dolomite and its implications for the formation of ancient dolomites. Geology 18 (5), 387–391.
- Veillard, C.M., John, C.M., Krevor, S., Najorka, J., 2019. Rock-buffered recrystallization of Marion Plateau dolomites at low temperature evidenced by clumped isotope thermometry and X-ray diffraction analysis. Geochim. Cosmochim. Acta 252, 190–212.
- Wei, H., Wang, X., Shi, X., Jiang, G., Tang, D., Wang, L., An, Z., 2019. Iodine content of the carbonates from the Doushantuo Formation and shallow ocean redox change on the Ediacaran Yangtze Platform, South China. Precambr. Res. 322, 160–169.
- Winkelbauer, H., Cordova-Rodriguez, K., Reyes-Macaya, D., Scott, J., Glock, N., Lu, Z., Hamilton, E., Chenery, S., Holdship, P., Dormon, C., Hoogakker, B., 2021. Foraminifera iodine to calcium ratios: approach and cleaning. Geochem. Geophys. Geosyst. 22 (11).
- Wong, G.T., Brewer, P.G., 1977. The marine chemistry of iodine in anoxic basins. Geochim. Cosmochim. Acta 41 (1), 151–159.
- Wörndle, S., Crockford, P.W., Kunzmann, M., Bui, T.H., Halverson, G.P., 2019. Linking the Bitter Springs carbon isotope anomaly and early Neoproterozoic oxygenation through I/[Ca+ Mg] ratios. Chem. Geol. 524, 119–135.
- Young, S.A., Kleinberg, A., Owens, J.D., 2019. Geochemical evidence for expansion of marine euxinia during an early Silurian (Llandovery-Wenlock boundary) mass extinction. Earth Planet. Sci. Lett. 513, 187–196.
- Zhang, S., DePaolo, D.J., 2020. Equilibrium calcite-fluid Sr/Ca partition coefficient from marine sediment and pore fluids. Geochim. Cosmochim. Acta 289, 33–46.
- Zhang, G., Lu, P., Zhang, Y., Tu, K., Zhu, C., 2020. SupPhreeqc: A program for generating customized Phreeqc thermodynamic datasets from Supcrtbl and extending calculations to elevated pressures and temperatures. Comput. Geosci. 143, 104560.
- Zhang, F., Xu, H., Konishi, H., Roden, E.E., 2010. A relationship between d 104 value and composition in the calcite-disordered dolomite solid-solution series. Am. Mineral. 95 (11–12), 1650–1656.
- Zhou, X., Thomas, E., Rickaby, R.E., Winguth, A.M., Lu, Z., 2014. I/Ca evidence for upper ocean deoxygenation during the PETM. Paleoceanography 29 (10), 964–975.
- Zhou, X., Jenkyns, H.C., Owens, J.D., Junium, C.K., Zheng, X.Y., Sageman, B.B., Hardisty, D.S., Lyons, T.W., Ridgwell, A., Lu, Z., 2015. Upper ocean oxygenation dynamics from I/Ca ratios during the Cenomanian-Turonian OAE 2. Paleoceanography 30 (5), 510–526.